MAPK activation may lead to successful strategies for targeting these molecules in the therapy of SARS.

Materials and methods

Cells and virus. Vero E6 cells were routinely subcultured in 75-cm^3 flasks in Dulbecco's modified Eagle's medium (DMEM, Sigma, St. Louis, MO, USA) supplemented with 0.2 mM L-glutamine, 100 U/ml penicillin, 100 μg/ml streptomycin, and 5% (v/v) fetal bovine serum (FBS), and maintained at 37 °C in an atmosphere of 5% CO_2. For use in the experiments, the cells were split once they reached 90% confluence and seeded onto 6-well or 24-well tissue culture plate inserts. The culture medium was changed to 2% FBS containing DMEM prior to virus infection. In this study, we used SARS-CoV [9], which was isolated as Frankfurt 1 [10] and kindly provided by Dr. J. Ziebuhr. The seed virus was passaged at least seven times, including one passage in our laboratory. Infection was usually performed with a multiplicity of infection (m.o.i.) of 5. The cells were stained with 0.05% crystal violet after fixing with 10% formaldehyde.

Anti-SARS-CoV antibodies. Two peptides, RYRIGNYKLNTD (GenBank Accession No. AAP13571; residues 197–208) and RRVRGGDGKMKE (GenBank Accession No. AAP13814; residues 93–194), corresponding to fragments of the amino acid sequences of membrane (M) and nucleocapsid (N) proteins of SARS-CoV, respectively, were synthesized (Sigma Genosys, Ishikari, Japan). Rabbits were injected with the mixture of peptides (New Drug Development Research Center, Iwamizawa, Japan), and the polyclonal rabbit antisera were used for Western blotting analysis.

Western blotting. After viral infection at an m.o.i. of 5, whole-cell extracts were electrophoresed in 10% and 10–20% gradient polyacrylamide gels, and transferred onto PVDF membrane sheets (Immobilon-P, Millipore, Bedford, MA, USA). In this study, we applied two sets of samples to polyacrylamide gels, and the membranes were divided into two sheets after blotting. The following antibodies, obtained from Cell Signaling Technology (Beverly, MA, USA), were used in this study at a dilution of 1:1000: rabbit anti-phospho p38 MAPK (Thr180/Tyr182), rabbit anti-p38, rabbit anti-phospho MAPKAPK-2 (Thr334), anti-MAPKAPK-2, rabbit anti-phospho HSP-27 (Ser82), mouse anti-HSP-27, mouse anti-phospho CREB (Ser133), rabbit anti-CREB, anti-phospho eIF4E (Ser209), and anti-rabbit eIF4E. Rabbit anti-actin (H-196) (diluted 1:200) was obtained from Santa Cruz Biotechnology (Santa Cruz, CA, USA). After 15-h incubation, the membranes were washed with 0.1% TBS–Tween and specific proteins were detected with a ProtoBlot II AP system (Promega, Madison, WI, USA), as described previously [11].

DNA fragmentation. A MEBCYTO Apoptosis ladder detection kit (Medical and Biological Laboratories, Nagoya, Japan) was used for detection of DNA fragmentation. After viral infection, cells were lysed with lysis buffer. The cellular DNA was precipitated with ethanol, dried, and resuspended in Tris–EDTA buffer (10 mM Tris, 1 mM EDTA, pH 7.5) containing 100 μg/ml RNase A. The DNA solutions were incubated for 60 min at 37 °C. The DNA was analyzed by electrophoresis on 1% agarose gels and then stained with ethidium bromide.

Results and discussion

Detection of SARS-CoV-specific proteins in virus-infected cells

Vero E6 cells were infected with SARS-CoV at an m.o.i. of 5, and Western blotting analysis was performed using polyclonal rabbit serum (see Materials and methods) and cellular extracts obtained at 6, 12, 18, and 24 h.p.i. Nucleocapsid (N) and membrane (M) proteins of SARS-CoV were detected after 6 and 12 h.p.i., respectively (Fig. 1). Multiple bands appeared on the Western blots, because the M proteins of coronavirus are glycosylated and the N proteins are phosphorylated in the virally infected cells. These bands were not observed in extracts from cells that were not infected by SARS-CoV, indicating that the polyclonal rabbit sera specifically detected SARS-CoV proteins.

SARS-CoV induces apoptosis in virus-infected cells

The cytopathic effect (CPE) caused by SARS-CoV is focal with cell rounding [12], and we were clearly able to observe such CPEs at 24 h.p.i. (Fig. 2A), while mouse hepatitis virus (MHV), a prototype of coronavirus, causes cell-fusion after infection, and MHV infection induces apoptotic cell death in murine 17Cl-1 cells [13]. To confirm whether SARS-CoV-infection induces apoptosis in Vero E6 cells, cellular DNA was extracted from SARS-CoV-infected cells. At 24 h.p.i., DNA fragmentation typical of apoptosis was observed (Fig. 2B). Avian coronavirus infectious bronchitis virus (IBV) also induces apoptosis in infected Vero cells.

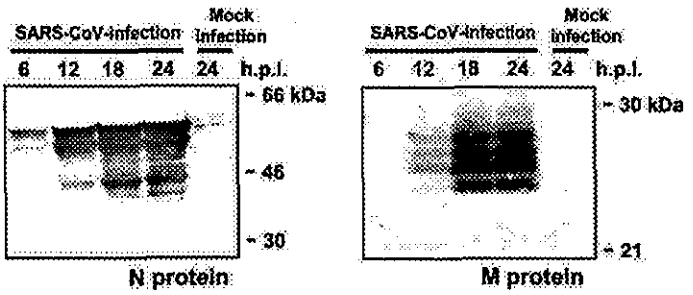

Fig. 1. Detection of SARS-CoV-specific proteins and activation of caspase-3 in virus-infected cells. Vero E6 cells were infected with SARS-CoV at an m.o.i. of 5, and Western blotting was then performed using proteins obtained at 6, 12, 18, and 24 h.p.i. Polyclonal antibodies against synthetic peptides based on membrane (M) and nucleocapsid (N) proteins were used.

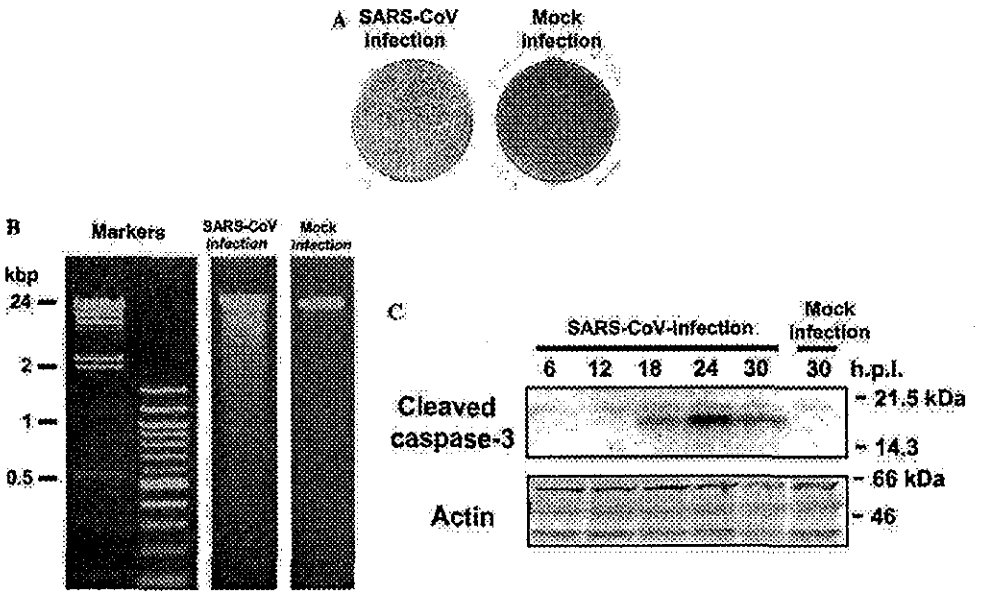

Fig. 2. Induction of apoptosis by SARS-CoV-infection. (A) Vero E6 cells were infected with SARS-CoV at an m.o.i. of 5 and stained with 0.05% crystal violet at 24 h.p.i. (B) DNA ladder fragmentation was detected at 24 h.p.i. (C) Western blotting analysis was performed using anti-cleaved caspase-3 antibody from 6, 12, 24, and 30 h.p.i. (C).

Caspase-3, which is one of the main effector caspases and is activated in response to both intracellular and extracellular death signals, was activated by IBV infection [14]. To confirm whether caspase-3 is activated by SARS-CoV-infection, Western blotting analysis was performed using anti-cleaved caspase-3 antibody. During apoptosis, caspase precursors are cleaved at Asp-X sites generating a large and a small subunit, which together constitute the active protease; the anti-caspase-3 antibody used in this study can specifically recognize the large fragment of cleaved caspase-3. As shown in Fig. 2C, the cleaved caspase-3 was detected in SARS-CoV-infected Vero E6 cells as a peak at 24 h.p.i. These results indicated that SARS-CoV induces apoptosis in the infected cells.

Activation of p38 MAPK in SARS-CoV-infected cells

Figs. 1 and 2 indicated that viral-specific proteins were synthesized at least 6 h.p.i., and the signaling pathway in response to stress should be activated from at least 6 to 24 h.p.i. by SARS-CoV-infection. Synthetic dsRNA poly(I)–poly(C) activates p38 MAPK and JNK/SAPK pathways in fibroblasts [15]: hence, double-stranded RNA intermediates of SARS-CoV that accumulate in infected cells may also trigger the p38 MAPK activation pathway. It was reported that p38 MAPK was activated in MHV-infected cells, and MHV replication has been shown to be necessary for p38 MAPK activation [7]. Therefore, the kinetics of p38 MAPK activation in SARS-CoV-infected Vero E6 cells were

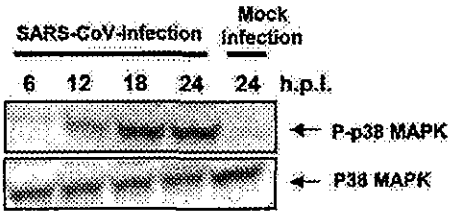

Fig. 3. Phosphorylation of p38 MAPK in SARS-CoV-infected Vero E6 cells. Phosphorylated and unphosphorylated p38 MAPK were detected by Western blotting analysis using proteins isolated from SARS-CoV-infected Vero E6 cells at 6, 12, 18, and 24 h.p.i.

analyzed. Vero E6 cells were infected with SARS-CoV at an m.o.i. of 5, and cell extracts were prepared at various times p.i. Western blotting analysis indicated an increase in the amount of phosphorylated p38 MAPK in the cells (Fig. 3). The p38 MAPK phosphorylation was not transient and reached the maximal level at 18 h.p.i. The role of p38 MAPK signaling pathway in cellular responses is diverse, depending on the cell type and stimulation. Thus, the p38 MAPK signaling pathway promotes both cell death and survival [16–18]. Therefore, investigation of the p38 MAPK-downstream targets is important to understand the mechanisms of cell death induced by SARS-CoV-infection.

MAPKAPK-2 and HSP-27 phosphorylation by SARS-CoV-infection

One of the downstream effectors of p38 MAPK is MAPK-activated protein kinase (MAPKAPK)-2, which

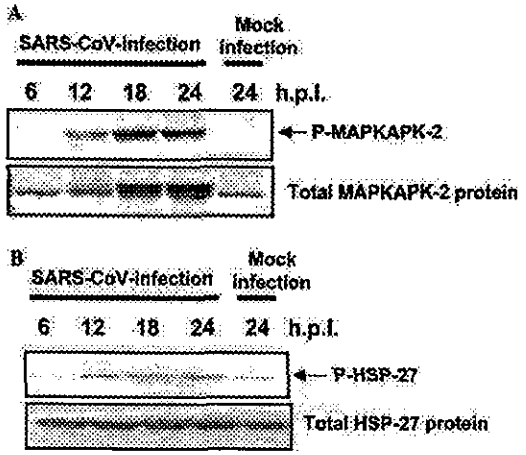

Fig. 4. Phosphorylation of MAPKAPK-2 and HSP-27 in virus-infected cells. (A) Phosphorylated and unphosphorylated MAPKAPK-2 were detected by Western blotting analysis. (B) Phosphorylated and unphosphorylated HSP-27 were detected by Western blotting analysis.

is activated in response to stress and growth factors [19,20]. We examined whether SARS-CoV-infection results in activation of this MAPKAPK-2 in Vero E6 cells. As shown in Fig. 4A, MAPKAPK-2 was phosphorylated in SARS-CoV-infected Vero E6 cells. To determine whether the substrates of MAPKAPK-2 are phosphorylated in the virus-infected cells, Western blotting analysis was performed using anti-phospho heat shock protein (HSP)-27. As shown in Fig. 4B, Hsp-27 was phosphorylated in SARS-CoV-infected cells at 12 h.p.i. A previous study showed that Hsp-27 has anti-apoptotic activity by inhibiting apoptosome formation [21].

Phosphorylation of transcription factors CREB and ATF-1

We next examined whether cAMP response element-binding protein (CREB), which is a substrate of mitogen- and stress-activated protein kinase (MSK)-1, was phosphorylated in infected cells. MSK-1 is thought to be a substrate of p38 MAPK and/or extracellular signal-related kinase (ERK)1/2. CREB was identified as an activator that responds to the cAMP-dependent signaling pathway and is also known to mediate an important survival signal under various conditions [22–24]. For example, the anti-apoptotic genes Bcl-2 and Bcl-xL are activated transcriptionally by phosphorylation of CREB in response to insulin-like growth factor (IGF)-I stimulation in PC-12 cells [25,26]. Immunoblot analysis (Fig. 5) indicated that the level of phosphorylated CREB was increased by SARS-CoV-infection. The anti-phospho CREB antibody used in this study also recognizes activation transcription factor (ATF)-1, which is a transcription factor. ATF-1 is a member of the CREB/ATF family that is phosphorylated by the cAMP-dependent protein kinase A (PKA) [27]. ATF-1 and CREB

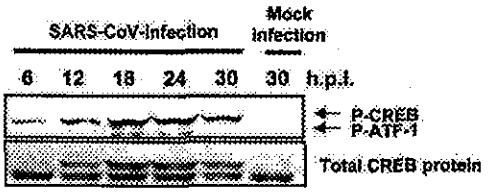

Fig. 5. Phosphorylation of CREB and ATF-1 in virus-infected cells. Phosphorylated and unphosphorylated CREB were detected by Western blotting analysis. Phosphorylated ATF-1 was also detected using anti-phospho CREB antibody.

act as survival factors [28]. This result suggested that phosphorylation of CREB and ATF-1 induces an anti-apoptotic environment in SARS-CoV-infected cells.

Phosphorylation of the translation initiation factor eIF4E

The translation initiation factor, eukaryotic initiation factor 4E (eIF4E), is phosphorylated by p38 MAPK and ERK1/2 [29,30], and eIF4E enhances translation rates of cap-containing mRNAs [31]. In the case of mouse hepatitis virus (MHV), eIF4E phosphorylation is utilized to promote virus-specific protein synthesis. Western blotting analysis was performed using anti-phospho eIF4E antibody. As shown in Fig. 6, the level of phosphorylated eIF4E was increased by SARS-CoV-infection.

Specific effective doses of p38 MAPK inhibitor

To confirm that the phosphorylation of downstream targets of p38 MAPK was specifically mediated by p38 MAPK, SB203580 (p38 MAPK-specific inhibitor), PD98059 (ERK1/2-specific inhibitor), and SP600125 (JNK-specific inhibitor) were used for inhibition of those function. Fifty percent confluency of Vero E6 cells were treated with 0, 10, 20, 30, 40, and 50 μM inhibitors in DMSO for 24, 48, and 72 h, and then cell viability was assayed using WST-1 system (Roche Diagnostics). Treating cells with up to 50 μM all inhibitors had little effect on cell viability (data not shown). Next, we examined the determination of specific inhibitory doses of

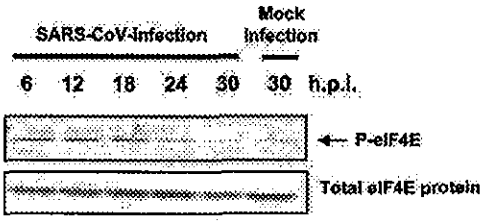

Fig. 6. Phosphorylation of eIF4E in virus-infected cells. Phosphorylated and unphosphorylated eIF4E were detected by Western blotting analysis.

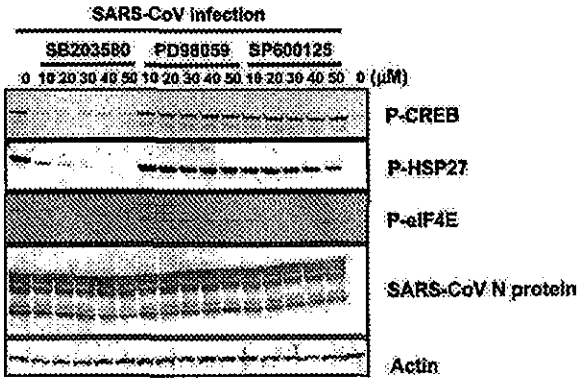

Fig. 7. Effective doses of p38 MAPK inhibitor. SARS-CoV-infected Vero E6 cells were treated with SB203580 (p38 MAPK-specific inhibitor), PD98059 (ERK1/2-specific inhibitor), and SP600125 (JNK-specific inhibitor) for 18 h. Western blot analysis was performed using anti-phosphorylated HSP-27, CREB eIF4E antibodies. SARS-CoV N protein was also detected.

p38 MAPK inhibitor in SARS-CoV-infected Vero E6 cells. SARS-CoV were infected to Vero E6 cells for 1 h, and then, three kinds of inhibitors were added to the cells. Proteins were harvested at 18 h.p.i. Western blot analysis was performed using anti-phospho CREB, HSP-27, and eIF4E antibodies (Fig. 7). The result shows that the eIF4E was effectively inhibited to be of phosphorylated type by p38 inhibitor between 10 and 50 μM. The effective dose for inhibition of CREB phosphorylation was more than 20 μM, and phosphorylated HSP-27 was not detected at 40 and 50 μM. Thus, this result indicated that CREB, HSP-27, and eIF4E were specifically phosphorylated by p38 MAPK, because both the ERK1/2 and JNK inhibitors did not inhibit those of phosphorylation between 10 and 50 μM. The 20 μM SB203580 was used in the study of MHV [7] and this concentration is known to efficiently block p38 MAPK activity in vivo [32]. Therefore, we used 20 and 30 μM SB 203580 in subsequent experiments.

No requirement for p38 MAPK phosphorylation of SARS-CoV replication

The p38 MAPK-dependent increase in eIF4E phosphorylation to promote virus-specific protein synthesis and subsequent progeny virus production were found in MHV [7]. Activated p38 MAPK and the downstream target, eIF4E, increased translation of MHV-specific proteins. We also found that eIF4E was activated in SARS-CoV-infection at 18 h.p.i. (Fig. 7). At that time of p.i., there was no significant difference in the amount of N protein of SARS-CoV among three inhibitor-treated cells and untreated cells. Kinetic study of N protein synthesis (Fig. 1A) showed that N protein seems to be the maximum amount in viral infected cells between 12 and 18 h.p.i. To investigate whether enhancement of virus-specific protein synthesis through virus-induced eIF4E activation occurs in SARS-CoV-infected cells, we tested the effect of p38 MAPK inhibitor, SB203580, on SARS-CoV-specific protein synthesis at early time p.i. Ten m.o.i. of SARS-CoV was inoculated in Vero E6 cells for 1 h, and then, the cells were washed two times. These cells were treated with 20 and 30 μM SB203580 for 6, 9, and 12 h.p.i. Western blot analysis showed that kinetics of SARS-CoV-specific protein accumulation in infected Vero E6 cells in the presence and absence of SB 203580 were similar (Fig. 8A). The phosphorylated eIF4E was detected at least 6 h.p.i. (Fig. 7) in SARS-CoV-infected cells. Taken together, SARS-CoV does not utilize activated eIF4E for its viral protein synthesis in Vero E6 cells. In addition, the CPEs caused by SARS-CoV-infection were slightly inhibited by SB203580 at late time p.i. (Fig. 8B).

In this study, we determined the cellular mechanisms by which SARS-CoV causes the activation of physiological intracellular signaling cascades that lead to the phosphorylation and activation of downstream molecules. We showed that SARS-CoV-infection of permissive cells induced the p38 MAPK signaling pathway. As

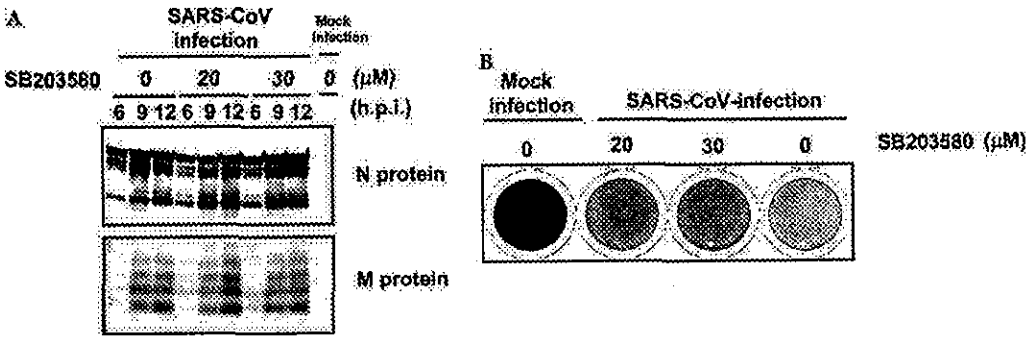

Fig. 8. Kinetics of N and M proteins synthesis in the presence of SB203580. After viral adsorption for 1 h, 20 and 30 μM of SB203580 was added to the cells. (A) Western blot analysis was performed at 6, 9, and 12 h.p.i. for detection of SARS-CoV N and M proteins. (B) Vero E6 cells were stained with 0.05% crystal violet at 41 h.p.i.

p38 MAPK is able to promote both cell death and survival [33], the substrates examined in this study and the other substrates of p38 MAPK may also induce cell death. Further studies are needed to determine which target molecules of p38 MAPK have inductive and preventative effects on apoptosis. To our knowledge, this is the first demonstration of activation of signaling transduction due to SARS-CoV-infection.

Acknowledgments

We thank Drs. F. Taguchi (National Institute of Infectious Diseases, Japan) for useful suggestions. We also thank Ms. M. Ogata (National Institute of Infectious Diseases, Japan) for her assistance. This work is partly supported by a grant-in-aid from the Ministry of Health, Labor and Welfare of Japan and Japan Health Science Foundation, Tokyo, Japan.

References

[1] P.A. Rota, M.S. Oberste, S.S. Monroe, W.A. Nix, R. Campagnoli, J.P. Icenogle, S. Penaranda, B. Bankamp, K. Maher, M.H. Chen, S. Tong, A. Tamin, L. Lowe, M. Frace, J.L. DeRisi, Q. Chen, D. Wang, D.D. Erdman, T.C. Peret, C. Burns, T.G. Ksiazek, P.E. Rollin, A. Sanchez, S. Liffick, B. Holloway, J. Limor, K. McCaustland, M. Olsen-Rasmussen, R. Fouchier, S. Gunther, A.D. Osterhaus, C. Drosten, M.A. Pallansch, L.J. Anderson, W.J. Bellini, Characterization of a novel coronavirus associated with severe acute respiratory syndrome, Science 300 (5624) (2003) 1394–1399.

[2] M.A. Marra, S.J. Jones, C.R. Astell, R.A. Holt, A. Brooks-Wilson, Y.S. Butterfield, J. Khattra, J.K. Asano, S.A. Barber, S.Y. Chan, A. Cloutier, S.M. Coughlin, D. Freeman, N. Girn, O.L. Griffith, S.R. Leach, M. Mayo, H. McDonald, S.B. Montgomery, P.K. Pandoh, A.S. Petrescu, A.G. Robertson, J.E. Schein, A. Siddiqui, D.E. Smailus, J.M. Stott, G.S. Yang, F. Plummer, A. Andonov, H. Artsob, N. Bastien, K. Bernard, T.F. Booth, D. Bowness, M. Czub, M. Drebot, L. Fernando, R. Flick, M. Garbutt, M. Gray, A. Grolla, S. Jones, H. Feldmann, A. Meyers, A. Kabani, Y. Li, S. Normand, U. Stroher, G.A. Tipples, S. Tyler, R. Vogrig, D. Ward, B. Watson, R.C. Brunham, M. Krajden, M. Petric, D.M. Skowronski, C. Upton, R.L. Roper, The genome sequence of the SARS-associated coronavirus, Science 300 (5624) (2003) 1399–1404.

[3] T.P. Garrington, G.L. Johnson, Organization and regulation of mitogen-activated protein kinase signaling pathways, Curr. Opin. Cell. Biol. 11 (1999) 211–218.

[4] A.J. Whitmarsh, R.J. Davis, A central control for cell growth, Nature 403 (2000) 255–256.

[5] L. Chang, M. Karin, Mammalian MAP kinase signalling cascades, Nature 410 (6824) (2001) 37–40.

[6] J.M. Kyriakis, J. Avruch, Mammalian mitogen-activated protein kinase signal transduction pathways activated by stress and inflammation, Physiol. Rev. 81 (2001) 807–869.

[7] S. Banerjee, K. Narayanan, T. Mizutani, S. Makino, Murine coronavirus replication-induced p38 mitogen-activated protein kinase activation promotes interleukin-6 production and virus replication in cultured cells, J. Virol. 76 (2002) 5937–5948.

[8] R. He, A. Leeson, A. Andonov, Y. Li, N. Bastien, J. Cao, C. Osiowy, F. Dobie, T. Cutts, M. Ballantine, X. Li, Activation of AP-1 signal transduction pathway by SARS coronavirus nucleocapsid protein, Biochem. Biophys. Res. Commun. 311 (2003) 870–876.

[9] C. Drosten, S. Gunther, W. Preiser, S. van der Werf, H.R. Brodt, S. Becker, H. Rabenau, M. Panning, L. Kolesnikova, R.A. Fouchier, A. Berger, A.M. Burguiere, J. Cinatl, M. Eickmann, N. Escriou, K. Grywna, S. Kramme, J.C. Manuguerra, S. Muller, V. Rickerts, M. Sturmer, S. Vieth, H.D. Klenk, A.D. Osterhaus, H. Schmitz, W. Doerr, Identification of a novel coronavirus in patients with severe acute respiratory syndrome, N. Engl. J. Med. 348 (20) (2003) 1967–1976.

[10] V. Thiel, K.A. Ivanov, A. Putics, T. Hertzig, B. Schelle, S. Bayer, B. Weissbrich, E.J. Snijder, H. Rabenau, H.W. Doerr, A.E. Gorbalenya, J. Ziebuhr, Mechanisms and enzymes involved in SARS coronavirus genome expression, J. Gen. Virol. 84 (2003) 2305–2315.

[11] T. Mizutani, M. Kobayashi, Y. Eshita, K. Shirato, T. Kimura, Y. Ako, H. Miyoshi, T. Takasaki, T. Kurane, H. Kariwa, T. Umemura, I. Takashima, Involvement of the JNK-like protein of the *Aedes albopictus* mosquito cell line, C6/36, in phagocytosis, endocytosis and infection of West Nile virus, Insect Mol. Biol. 12 (2003) 491–499.

[12] T.G. Ksiazek, D. Erdman, C.S. Goldsmith, S.R. Zaki, T. Peret, S. Emery, S. Tong, C. Urbani, J.A. Comer, W. Lim, P.E. Rollin, S.F. Dowell, A.E. Ling, C.D. Humphrey, W.J. Shieh, J. Guarner, C.D. Paddock, P. Rota, B. Fields, J. DeRisi, J.Y. Yang, N. Cox, J.M. Hughes, J.W. LeDuc, W.J. Bellini, L.J. Anderson, SARS working group. A novel coronavirus associated with severe acute respiratory syndrome, N. Engl. J. Med. 348 (20) (2003) 1953–1966.

[13] C.J. Chen, S. Makino, Murine coronavirus-induced apoptosis in 17Cl-1 cells involves a mitochondria-mediated pathway and its downstream caspase-8 activation and bid cleavage, Virology 302 (2002) 321–332.

[14] C. Liu, H.Y. Xu, D.X. Liu, Induction of caspase-dependent apoptosis in cultured cells by the avian coronavirus infectious bronchitis virus, J. Virol. 75 (2001) 6402–6409.

[15] M.S. Iordanov, J.M. Paranjape, A. Zhou, J. Wong, B.R. Williams, E.F. Meurs, R.H. Silverman, B.E. Magun, Activation of p38 mitogen-activated protein kinase and c-Jun NH_2-terminal kinase by double-stranded RNA and encephalomyocarditis virus: involvement of RNase L, protein kinase R, and alternative pathways, Mol. Cell. Biol. 20 (2000) 617–627.

[16] N. Juretic, J.F. Santibanez, C. Hurtado, J. Martinez, ERK 1,2 and p38 pathways are involved in the proliferative stimuli mediated by urokinase in osteoblastic SaOS-2 cell line, J. Cell. Biochem. 83 (2001) 92–98.

[17] B. Liu, M. Fang, Y. Lu, G.B. Mills, Z. Fan, Involvement of JNK-mediated pathway in EGF-mediated protection against paclitaxel-induced apoptosis in SiHa human cervical cancer cells, Br. J. Cancer 85 (2001) 303–311.

[18] G. Yosimichi, T. Nakanishi, T. Nishida, T. Hattori, T. Takano-Yamamoto, M. Takigawa, CTGF/Hcs24 induces chondrocyte differentiation through a p38 mitogen-activated protein kinase (p38MAPK), and proliferation through a p44/42 MAPK/extracellular-signal regulated kinase (ERK), Eur. J. Biochem. 268 (2001) 6058–6065.

[19] I.N. Foltz, J.C. Lee, P.R. Young, J.W. Schrader, Hemopoietic growth factors with the exception of interleukin-4 activate the p38 mitogen-activated protein kinase pathway, J. Biol. Chem. 272 (1997) 3296–3301.

[20] N.W. Freshney, L. Rawlinson, F. Guesdon, E. Jones, S. Cowley, J. Hsuan, J. Saklatvala, Interleukin-1 activates a novel protein kinase cascade that results in the phosphorylation of Hsp27, Cell 78 (1994) 1039–1049.

[21] C. Garrido, E. Schmitt, C. Cande, N. Vahsen, A. Parcellier, G. Kroemer, HSP27 and HSP70: potentially oncogenic apoptosis inhibitors, Cell Cycle 2 (2003) 579–584.

[22] Y. Tan, J. Rouse, A. Zhang, S. Cariati, P. Cohen, M.J. Comb, FGF and stress regulate CREB and ATF-1 via a pathway involving p38 MAP kinase and MAPKAP kinase-2, EMBO J. 15 (1996) 4629–4642.
[23] D.D. Ginty, A. Bonni, M.E. Greenberg, Nerve growth factor activates a Ras-dependent protein kinase that stimulates c-fos transcription via phosphorylation of CREB, Cell 77 (1994) 713–725.
[24] A. von Knethen, A. Lotero, B. Brune, Etoposide and cisplatin induced apoptosis in activated RAW 264.7 macrophages is attenuated by cAMP-induced gene expression, Oncogene 17 (1998) 387–394.
[25] S. Pugazhenthi, T. Boras, D. O'Connor, M.K. Meintzer, K.A. Heidenreich, J.E. Reusch, Insulin-like growth factor I-mediated activation of the transcription factor cAMP response element-binding protein in PC12 cells. Involvement of p38 mitogen-activated protein kinase-mediated pathway, J. Biol. Chem. 274 (1999) 2829–2837.
[26] M. Parrizas, D. LeRoith, Specific inhibition of insulin-like growth factor-1 and insulin receptor tyrosine kinase activity and biological function by tyrphostins, Endocrinology 138 (1997) 1355–1358.
[27] K.A. Lee, N. Masson, Transcriptional regulation by CREB and its relatives, Biochim. Biophys. Acta 1174 (1993) 221–233.
[28] D. Jean, M. Harbison, D.J. McConkey, Z. Ronai, M. Bar-Eli, CREB and its associated proteins act as survival factors for human melanoma cells, J. Biol. Chem. 273 (1998) 24884–24890.
[29] S.J. Morley, L. McKendrick, Involvement of stress-activated protein kinase and p38/RK mitogen-activated protein kinase signaling pathways in the enhanced phosphorylation of initiation factor 4E in NIH 3T3 cells, J. Biol. Chem. 272 (1997) 17887–17893.
[30] S. Pyronnet, H. Imataka, A.C. Gingras, R. Fukunaga, T. Hunter, N. Sonenberg, Human eukaryotic translation initiation factor 4G (eIF4G) recruits mnk1 to phosphorylate eIF4E, EMBO J. 18 (1999) 270–279.
[31] A.C. Gingras, B. Raught, N. Sonenberg, eIF4 initiation factors: effectors of mRNA recruitment to ribosomes and regulators of translation, Annu. Rev. Biochem. 68 (1999) 913–963.
[32] A. Cuenda, D.R. Alessi, Use of kinase inhibitors to dissect signaling pathways, Methods Mol. Biol. 99 (2000) 161–175.
[33] P. Dent, A. Yacoub, P.B. Fisher, P.M.P. Hagan, S. Grant, MAPK pathways in radiation responses, Oncogene 22 (2003) 5885–5896.

FEBS 28924 FEBS Letters 577 (2004) 187–192

Tyrosine dephosphorylation of STAT3 in SARS coronavirus-infected Vero E6 cells

Tetsuya Mizutani[a,*], Shuetsu Fukushi[a], Masaaki Murakami[b], Toshio Hirano[b], Masayuki Saijo[a], Ichiro Kurane[a], Shigeru Morikawa[a]

[a] *Special Pathogens Laboratory, Department of Virology 1, National Institute of Infectious Diseases, Gakuen 4-7-1, Musashimurayama, Tokyo 208-0011, Japan*
[b] *Department of Molecular Oncology, Graduate School of Medicine, Graduate School of Frontier Biosciences, Osaka University, Suita, Osaka, Japan*

Received 23 July 2004; revised 27 September 2004; accepted 4 October 2004

Available online 14 October 2004

Edited by Hans-Dieter Klenk

Abstract **Severe acute respiratory syndrome (SARS) has become a global public health emergency. p38 mitogen-activated protein kinase (MAPK) and its downstream targets are activated in SARS coronavirus (SARS-CoV)-infected Vero E6 cells and activation of p38 MAPK enhances the cytopathic effects of SARS-CoV infection. In addition, weak activation of Akt cannot prevent SARS-CoV infection-induced apoptosis in Vero E6 cells. In the present study, we demonstrated that signal transducer and activator of transcription (STAT) 3, which is constitutively phosphorylated at tyrosine (Tyr)-705 and slightly phosphorylated at serine (Ser)-727 in Vero E6 cells, was dephosphorylated at Tyr-705 on SARS-CoV infection. In addition to phosphorylation of p38 MAPK in virus-infected cells, other MAPKs, i.e., extracellular signal-regulated kinase (ERK) 1/2 and c-Jun N-terminal kinase (JNK), were phosphorylated. Although inhibitors of ERK1/2 and JNK (PD98059 and SP600125) had no effect on phosphorylation status of STAT3, inhibitors of p38 MAPK (SB203580 and SB202190) partially inhibited dephosphorylation of STAT3 at Tyr-705. Tyr-705-phosphorylated STAT3 was localized mainly in the nucleus in mock infected cells, whereas STAT3 disappeared from the nucleus in virus-infected cells. As STAT3 acts as an activator of transcription in the nucleus, these results suggest that STAT3 lacks its activity on transcription in SARS-CoV-infected Vero E6 cells.**

Keywords: Severe acute respiratory syndrome coronavirus; Signal transducer and activator of transcription 3; p38; Extracellular signal-regulated kinase 1/2; c-Jun N-terminal kinase

1. Introduction

Severe acute respiratory syndrome (SARS) is a newly found infectious disease caused by a novel coronavirus, SARS coronavirus (SARS-CoV) [1,2]. In late 2002, SARS-CoV spread from Guangdong Province in China to more than 30 countries. The pathogenesis of SARS in vivo may be mediated by both the effect of viral replication in the target cells and immune responses. Recently, we reported that p38 mitogen-activated protein kinase (MAPK) plays important roles in the cytopathic effects and apoptosis in SARS-CoV-infected cells [3]. Furthermore, weak activation of Akt cannot prevent apoptosis by SARS-CoV-infection [4]. Thus, it is necessary to examine the signaling pathways in SARS-CoV-infected cells in culture to understand the molecular mechanisms of its pathology in vivo.

MAPKs are signal transducers that respond to extracellular stimulation by cytokines, growth factors, viral infection, and stressors, and in turn regulate cell differentiation, proliferation, survival, and apoptosis [5–8]. p38 MAPK is strongly activated by stressors and inflammatory cytokines. Our previous study indicated that p38 MAPK phosphorylation in SARS-CoV-infected Vero E6 cells reached the maximal level at 18 h post-infection (h.p.i.) and cytopathic effects (CPEs) were observed from 24 h.p.i. [3]. The CPEs were partially prevented by treatment with the p38 MAPK inhibitor SB203580, strongly suggesting that the p38 MAPK signaling pathway is involved in the control of cell death in SARS-CoV-infected Vero E6 cells. On the other hand, signal transducer and activator of transcription (STAT) proteins are transcription factors that mediate cytokines and growth factors. Activation of all STAT proteins is induced by phosphorylation of a single tyrosine residue, leading to dimerization via an intermolecular SH2 phosphotyrosine interaction [9–12]. STAT3 is a major transcription factor activated in response to cytokines, such as interleukin-6 (IL-6) and IL-10. Inhibition of STAT3 signaling by dominant negative and antisense STAT3 inhibitors resulted in a decrease in cell viability and subsequent apoptosis [13–15]. Thus, STAT3 is thought to act as an anti-apoptotic transcription factor. Recent studies indicated that interactions between STATs and some viral proteins cause degradation of STATs in virus-infected cells. For example, V protein of measles virus forms complexes with STAT1, STAT2, and STAT3, and inhibits extracellular (IL-6) and intracellular (v-Src) STAT3-dependent signaling [16]. Thus, measles virus-induced degradation of STATs may provide a mechanism for virus-induced cytokine inhibition that links innate immune evasion to adaptive immune suppression.

In the present study, we found that STAT3, constitutively phosphorylated at tyrosine (Tyr)-705 and slightly phosphorylated at serine (Ser)-727 in Vero E6 cells, was dephosphorylated at Tyr-705 by activation of p38 MAPK on SARS-CoV infection. Lack of transcriptional activity of STAT3 by viral infection may decrease anti-apoptotic activity in the cells.

* Corresponding author. Fax: +81-42-564-4881.
E-mail address: tmizutan@nih.go.jp (T. Mizutani).

0014-5793/$22.00
doi:10.1016/j.febslet.2004.10.005

2. Materials and methods

2.1. Cells and virus

Vero E6 cells were routinely subcultured in 75-cm^3 flasks in Dulbecco's modified Eagle's medium (DMEM, Sigma, St. Louis, MO, USA) supplemented with 0.2 mM L-glutamine, 100 units/ml penicillin, 100 μg/ml streptomycin, and 5% (v/v) fetal bovine serum (FBS), and maintained at 37 °C in an atmosphere of 5% CO_2. For use in the experiments, the cells were split once onto 6- or 24-well tissue culture plate inserts and cultured until they reached 100% confluence. The culture medium was changed to 2% FBS containing DMEM prior to virus infection. SARS-CoV, which was isolated as Frankfurt 1 [17] and kindly provided by Dr. J. Ziebuhr, was used in the present study. Infection was usually performed with a multiplicity of infection (m.o.i.) of 10.

2.2. Treatment with inhibitors

SB203580 and SB202190 as p38 MAPK inhibitors, PD098059 as a MEK inhibitor and SP600125 as a JNK inhibitor were dissolved in dimethyl sulfoxide (DMSO) at a concentration of 10 or 20 mM. All reagents were purchased from Calbiochem (San Diego, CA, USA). All test wells, including mock treated controls, were treated with 0.25% DMSO (v/v). Vero E6 cells were inoculated with SARS-CoV at m.o.i. of 10 for 1 h and then cells were treated with inhibitors for 17 h.

2.3. Subcellular fractionation

SARS-CoV-infected or mock infected Vero E6 cells at 18 h.p.i. were subjected to subcellular fractionation using a Subcellular Proteome Extraction Kit (Calbiochem) according to the manufacturer's instructions. Each subcellular fraction was then analyzed by Western blotting.

2.4. Western blotting

After virus infection, whole-cell extracts were electrophoresed on either 12.5% or 10–20% gradient polyacrylamide gels and transferred onto PVDF membranes (Immobilon-P, Millipore, Bedford, MA, USA). In the present study, we applied two sets of samples to polyacrylamide gels and the membranes were divided into two halves after blotting. The following antibodies, obtained from Cell Signaling Technology Inc. (Beverly, MA, USA), were used in the present study at a dilution of 1:1000: rabbit anti-phospho STAT3 (Tyr-705) antibody, rabbit anti-phospho STAT3 (Ser-727) antibody, rabbit anti-p38 MAPK (Thr180/Tyr182) antibody, rabbit anti-p38 MAPK antibody, rabbit anti-phospho p44/42 MAPK (Thr202/Tyr204) (=ERK1/2) antibody, rabbit anti-p44/42 MAPK (=ERK1/2) antibody, rabbit anti-phospho SAPK/JNK (Thr183/Tyr185) antibody, anti-SAPK/JNK antibody, anti-phospho MEK1/2 (Ser217/221) antibody, anti-MEK1/2 antibody, anti-phospho SEK1/MKK4 (Thr261) antibody, anti-SEK1/MKK4 antibody, anti-phospho MKK7 (Ser271/Thr275) antibody, anti-MKK7 antibody, anti-phospho MKK3/MKK6 (Ser189/207) antibody, anti-MKK3 antibody, anti-phospho Jak1 (Tyr1022/1023) an- tibody, anti-phospho JAK2 (Tyr1007/1008) antibody, and anti-phospho Tyk2 (Tyr1054/1055) antibody. Mouse anti-STAT3 antibody (diluted 1:2500), mouse anti-JAK1 antibody (diluted 1:250), and mouse anti-Tyk2 antibody (diluted 1:1000), obtained from BD Biosciences, Franklin Lakes, NJ, USA, were also used. Rabbit anti-JAK2 antibody (C-20, diluted 1:200) was obtained from Santa Cruz Biotechnology (Santa Cruz, CA, USA). After 15-h incubation with the above antibodies, the membranes were washed with Tris-borate saline containing 0.1% Tween 20 (0.1% TBS-Tween) and the reactions were detected with a ProtoBlot II AP system (Promega Co., Madison, WI, USA), as described previously [18].

3. Results

3.1. Tyrosine dephosphorylation of STAT3 in SARS-CoV-infected cells

As described in our previous report, we compared the cellular protein profiles of SARS-CoV-infected (18 h.p.i. when apoptosis was not evident) and mock infected Vero E6 cells by Western blotting using 125 antibodies to investigate cellular responses to SARS-CoV-infection [3,4]. Cellular proteins related to several signaling pathways that responded specifically to SARS-CoV infection, including p38 MAPK and Akt, were found. In the present study, we examined whether signal transducer and activator of transcription 3 (STAT3) was dysregulated on infection with SARS-CoV, as reported for measles virus-infection [16]. Vero E6 cells were infected with SARS-CoV at m.o.i. of 10, and cellular proteins were harvested at 6, 12, 18, and 24 h.p.i. Western blotting analysis was performed using a series of anti-STAT3 antibodies that recognized total STAT3 or Tyr-705- or Ser-727-phosphorylated forms of STAT3. In Vero E6 cells, STAT3 was phosphorylated constitutively at Tyr-705, whereas Ser-727 was only slightly phosphorylated (Fig. 1; mock infection). Constitutive activation of STAT3 was observed in breast carcinoma cell lines [19]. Interestingly, Tyr-705-phosphorylated STAT3 was not detected after 18 h.p.i. in SARS-CoV-infected Vero E6 cells, even though the total amount of STAT3 did not change until 24 h.p.i. (Fig. 1). This result suggested that STAT3 Tyr-705 was dephosphorylated from 18 to 24 h.p.i. On the other hand, Ser-727-phosphorylated STAT3 was slightly increased at the same time points. Based on the hypothesis that tyrosine phosphorylation of STAT is necessary for its activation [9–12], these results suggest that the level of activation of STAT3 was decreased in SARS-CoV-infected Vero E6 cells. Thus, the mechanism of dysregulation of STAT3 by SARS-CoV is different from that by measles virus in which Measles virus V protein forms complexes with STATs resulting in degradation of STAT3.

3.2. Phosphorylation level of upstream kinases of STAT3

As a general explanation of signal transduction of STAT3, binding of IL-6 to the receptor induces dimerization of the common gp130 signal transduction subunit of the IL-6 family of cytokine receptors, and then Janus kinases (JAK1 and 2) and Tyk2 are phosphorylated at tyrosine residues through a conserved membrane-proximal binding domain [20]. The phosphorylated JAKs and Tyk2 create docking sites for STAT3. Dimeric STAT3 Tyr-phosphorylated by JAKs and Tyk2 migrates to the nucleus, where STAT3 activates transcription of specific genes. Thus, JAK1, JAK2, Tyk2, and STAT3 are phosphorylated in response to IL-6. To test the hypothesis that Tyr-705-dephosphorylation of STAT3 by SARS-CoV infection occurred due to a lack of signals from JAK1/2 and Tyk2, the phosphorylation status of these kinases was examined in virus-infected or mock infected Vero E6 cells. As shown in Fig. 2, JAK1, JAK2, and Tyk2 were phosphor-

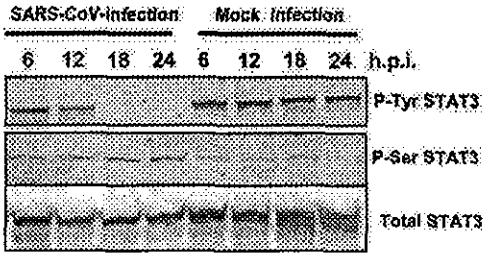

Fig. 1. Infection of Vero E6 cells with SARS-CoV affected the signaling pathway of STAT3. Western blotting analysis of proteins from SARS-CoV-infected Vero E6 cells was performed using antibodies that recognized forms of STAT3 phosphorylated at Tyr-705 or Ser-727.

ylated at low levels in mock infected cells, whereas no significant changes in phosphorylation level of these kinases were observed after virus infection. These observations suggest that Tyr-705 dephosphorylation of STAT3 in virus-infected cells occurred independent of its upstream kinases. Therefore, total activity of STAT3 may be low in Vero E6 cells. However, it can not be ruled out that the anti-phospho JAK1, JAK2 and Tyk2 antibodies used in the present study are difficult to be recognized in the phosphorylated JAK1, JAK2 and Tyk2 in Vero E6 cells as the datasheet included no description of cross-reactivity with monkey.

3.3. Stimulation of Tyr-705 phosphorylation of STAT3 by cytokines

Previous studies have indicated that at least six cytokines, IL-2, IL-6, IL-10, IL-15, IL-17, and IL-22, can stimulate activation of STAT3 [21–24]. Tyr-705 dephosphorylation of STAT3 in virus-infected cells may be due to a lack of stimulation by these cytokines after 18 h.p.i. Therefore, it is important to identify the cytokines responsible for stimulating Tyr phosphorylation of STAT3 to understand the mechanism of Tyr-705-dephosphorylation of STAT3 in virus-infected cells. To investigate whether fetal calf serum (FCS) in the medium contains stimulators for STAT3 phosphorylation, Vero E6 cells were cultured in DMEM containing 0%, 2% or 5% FCS for 18 h, subjected to subcellular fractionation, and then the proteins were analyzed by Western blotting using anti-phospho-specific antibodies. As shown in Fig. 3A, there were no significant differences in total amount of STAT3 in cultures with various concentrations of FCS in the medium. This result suggests that FCS does not contain components that stimulate Tyr-phosphorylation of STAT3. We next determined cytokines and their receptors produced in Vero E6 cells using a GEArray Q Series Human Interleukin and Receptor Gene Array (SuperArray Bioscience Corporation, Frederick, MD, USA). Expression level of IL-22, which has also been reported as a stimulator of STAT3 [23], was very low, and receptors for IL-22 (IL-22RA1 and RA2) were obtained as strong and weak signals, respectively (data not shown). Therefore, we examined whether IL-22 stimulated Tyr-705 and Ser-727 phosphorylation of STAT3. As shown in Fig. 4A, the level of Tyr-705-phosphorylated STAT3 increased 15 min after treatment with murine IL-22 (200 ng/ml) (Pepro Tech EC, London, UK), whereas phosphorylation of Ser-727 was not enhanced, suggesting that it is difficult for Ser-727 of

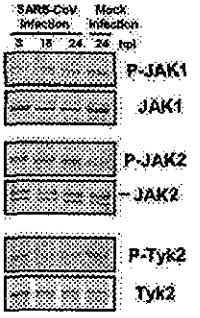

Fig. 2. Phosphorylation levels of upstream kinases of STAT3 in virus-infected cells. Western blotting analyses were performed using anti-phospho JAK1, JAK2, and Tyk2 antibodies.

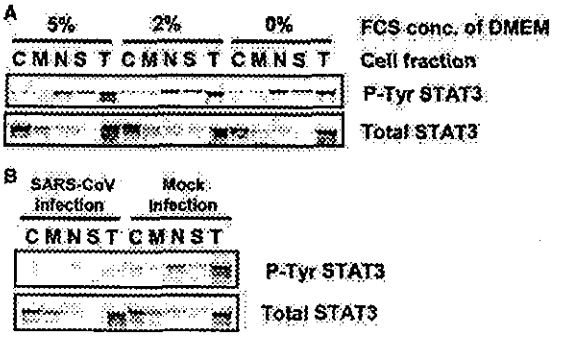

Fig. 3. Subcellular localization of Tyr-phosphorylated STAT3. (A) Vero E6 cells were incubated in DMEM containing 0%, 2% or 5% FCS for 18 h. After subcellular fractionation, Western blotting was performed using anti-phospho STAT3 (Tyr) antibody. (B) C, M, N, S, and T indicate cytosolic, organelle/membrane, nuclear, cytoskeletal, and total cellular fraction, respectively.

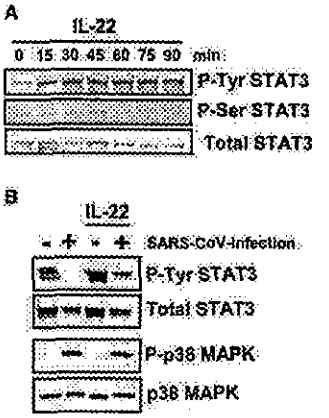

Fig. 4. IL-22 induces Tyr phosphorylation of STAT3. (A) Vero E6 cells were treated with IL-22 from 0 to 90 min. Cellular proteins were sampled every 15 min. Western blotting was performed using anti-phospho STAT3 (Tyr and Ser) antibodies. (B) SARS-CoV-infected Vero E6 cells were treated with IL-22 for 20 min at 18 h.p.i., and then, Western blot analysis was performed using anti-phospho STAT3 (Tyr) and anti-phospho p38 MAPK.

STAT3 to be phosphorylated in Vero E6 cells stimulated by SARS-CoV infection and IL-22. Although the phosphorylation level of p38 MAPK was not changed in SARS-CoV-infected Vero E6 cells by treatment with IL-22 for 20 min at 18 h.p.i., the Tyr-705-phosphorylation of STAT3 increased (Fig. 4B). These results suggest that signaling pathway via IL-22 is not regulated by p38 MAPK in Vero E6 cells.

3.4. Tyr-705-phosphorylated STAT3 in the nucleus

To determine the localization of Tyr-705-phosphorylated STAT3 in Vero E6 cells, subcellular extraction was performed using a Subcellular Proteome Extraction Kit (Calbiochem) and then Western blotting analyses were performed. As described above, the amounts of total and Tyr-705-phosphorylated STAT3 were similar in cells grown in media containing 0%, 2% or 5% FCS. The subcellular localization of STAT3 was not

affected by the concentration of FCS (Fig. 3A). Total STAT3 was located mainly in the cytosol, and also in membranes/organelles and the nuclear fractions. On the other hand, Tyr-705-phosphorylated STAT3 appeared mainly in the nuclear fraction. We next examined whether Tyr-705-phosphorylated STAT3 was not present in the nucleus in SARS-CoV-infected Vero E6 cells at 18 h.p.i. As shown in Fig. 3B, Tyr-705-phosphorylated STAT3 had clearly disappeared from the nuclear fraction in virus-infected cells. This result strongly suggested that STAT3 did not act as a transcriptional enhancer in SARS-CoV-infected Vero E6 cells after 18 h.p.i.

3.5. Phosphorylation of MAPKs in SARS-CoV-infected cells

Our previous report indicated that SARS-CoV-infection to Vero E6 induced phosphorylation of p38 MAPK and its downstream targets, HSP-27, eIF4E and CREB [3]. Phosphorylation of these proteins was prevented by treatment of the cells with the p38 MAPK inhibitor SB20854. MAPKs were reported to induce Ser-727 phosphorylation of STAT3 [25]. To investigate whether other MAPKs, i.e., ERK1/2 (extracellular signal-regulated kinase) and JNK, are also phosphorylated in SARS-CoV-infected Vero E6 cells, the kinetics of phosphorylation of ERK1/2 and JNK were analyzed by Western blotting. Vero E6 cells were infected with SARS-CoV at m.o.i. of 10 and the cell extracts were prepared at various time points after infection. Western blotting analysis demonstrated that levels of phosphorylated ERK1/2 and JNK were increased in SARS-CoV-infected cells (Fig. 5A). Two phosphorylated forms of ERK, ERK1 and ERK2, were detected at 12 h.p.i. and accumulated continuously up to 24 h.p.i. The kinetics of accumulation of phosphorylated ERK1/2 and JNK in the infected cells were similar to that of accumulation of phosphorylated p38 MAPK. We next examined whether the upstream MAPK kinases (MAPKKs) were also phosphorylated in SARS-CoV-infected Vero E6 cells. The kinases of p38, ERK1/2, and JNK are known as MKK3/6, MEK1/2, and MKK4/7, respectively. As shown in Fig. 5, MKK3/6, MEK1/2, and MKK4/7 were phosphorylated in SARS-CoV-infected Vero E6 cells.

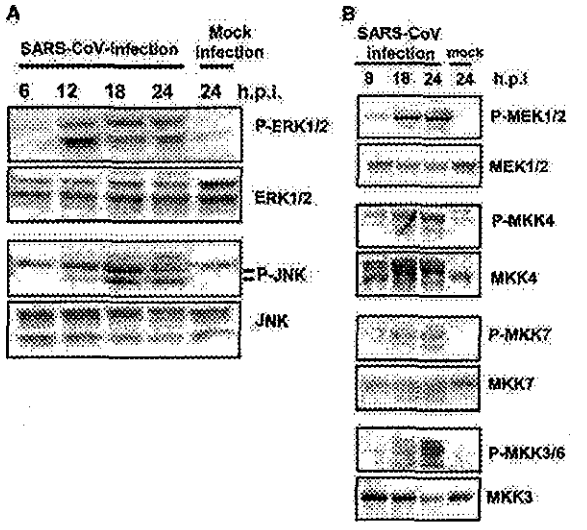

Fig. 5. MAPKs phosphorylation in virus-infected cells. Western blotting analysis of proteins from SARS-CoV-infected Vero E6 cells was performed using anti-phospho ERK1/2, JNK, MEK1/2, MKK4, MKK7, and MKK3/6 antibodies.

3.6. Tyr dephosphorylation of STAT3 by p38 MAPK

To investigate whether Tyr-705 phosphorylation is regulated by activated MAPKs in SARS-CoV-infected Vero E6 cells, the infected cells were treated for 18 h with three MAPK inhibitors: SB203580 (p38 MAPK inhibitor), PD98059 (MEK inhibitor), and SP600125 (JNK inhibitor). Tyr-705- and Ser-727-phosphorylated STAT3 were then analyzed by Western blotting. As shown in Fig. 6A, SB203580 did not affect Ser-727 phosphorylation of STAT3, while SARS-CoV-induced dephosphorylation of STAT3 Tyr-705 was partially inhibited by SB203580. On the other hand, neither PD98059 nor SP600125 affected STAT3 phosphorylation. To confirm whether inhibition of p38 prevents dephosphorylation of STAT3 Tyr-705, virus-infected cells were treated with another p38 inhibitor, SB202190. As shown in Fig. 6B, Tyr-705 dephosphorylation of STAT3 in the infected cells was also partially inhibited by SB202190. These results indicated that activated p38 MAPK in SARS-CoV-infected Vero E6 cells regulates Tyr-705 phosphorylation of STAT3, but not that of Ser-727.

4. Discussion

In the present and previous studies, we reported that the cellular mechanisms by which SARS-CoV caused the activation of physiological intracellular signaling cascades that lead to the phosphorylation and activation of downstream molecules [3,4]. We showed here that SARS-CoV-infection of permissive Vero E6 cells stimulated p38, ERK1/2, and JNK

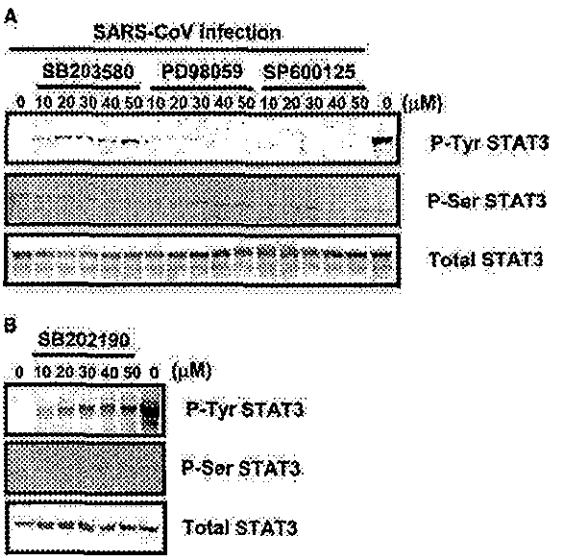

Fig. 6. Effects of treatment of SARS-CoV-infected Vero E6 cells with p38 MAPK inhibitor. (A) Vero E6 cells were infected with SARS-CoV at m.o.i. of 10, and then incubated with SB203580, PD98059, and SP600125 at concentrations from 10 to 50 μM for 17 h. Western blotting analyses were performed to detect Tyr-705- and Ser-727-phosphorylated forms of STAT3. (B) SB202190 was used as a p38 MAPK inhibitor.

signaling pathways. The activation of p38 MAPK induces cytopathic effects in Vero E6 cells, whereas ERK1/2 and JNK had no effect (unpublished data). As MAPKKs for p38, ERK1/2, and JNK were all phosphorylated in virus-infected cells, further studies are needed to identify triggers of the stress-activated response pathway by viral infection. The present study strongly suggested that the p38 MAPK signaling pathway is upstream of Tyr-705 dephosphorylation of STAT3. We also demonstrated that infection with SARS-CoV slightly increased the level of phosphorylation of Ser-727 STAT3. Although the effect of Ser-727 phosphorylation on the function of STAT3 in SARS-CoV-infected cells remains unresolved, a previous study showed that phosphorylation of Ser-727 of STAT3 negatively modulates its tyrosine phosphorylation [26]. Thus, the timing of Tyr-705 dephosphorylation and Ser-727 phosphorylation may be almost the same in SARS-CoV-infected cells. The Ser-727-phosphorylated STAT3-mediated expression of a Bcl-2 family member, Mcl-1, is essential for the survival of cells [27], suggesting that Ser-727-phosphorylated STAT3 has anti-apoptotic activity. However, the mechanism through which serine phosphorylation regulates the transcriptional activities of STAT3 is still unclear. On the other hand, one of the important roles of Tyr-705-phosphorylated STAT3 is binding to regulatory DNA elements that control the expression of target genes [28,29]. Suppression of STAT3 expression by siRNA induces apoptosis in several astrocytoma cell lines, and STAT3 is required for the expression of the anti-apoptotic genes survivin and Bcl-xL in the A172 glioblastoma cell line [30]. In addition, the role of STAT proteins during viral infection has been the subject of several recent studies. The proteasome-dependent degradation of STAT1 is induced by V protein of simian virus 5 [31], while type II human parainfluenza virus V protein targets STAT2, and mumps virus V protein targets both STAT1 and STAT3 [32–34]. In measles virus-infected cells, the V protein forms complexes with STAT1, STAT2, and STAT3, and inhibits both IL-6- and v-Src STAT3-dependent signaling [16]. Thus, a role of V protein as an inhibitor of the STAT3 signaling pathway is advantageous for viral growth. SARS-CoV may also obtain a growth advantage by Tyr-705 dephosphorylation of STAT3.

Our recent study indicated that Akt was also activated in response to SARS-CoV-replication [4]. Although phosphorylation of serine residue 473 on Akt was detected at least 8 h.p.i., threonine residue 308 was not phosphorylated in virus-infected Vero E6 cells. A downstream target of Akt, glycogen synthase kinase 3β (GSK-3β), was slightly phosphorylated, indicating that the level of activation of Akt was very low. The present study showed that IL-22 can induce Tyr-705 phosphorylation of STAT3, but not Ser-727 phosphorylation, similarly to SARS-CoV infection. It may be difficult for Ser-727 of STAT3 to be phosphorylated in Vero E6 cells, similarly to Thr-308 of Akt. Based on these results, we hypothesized that weak activation of Akt cannot prevent apoptosis induced by SARS-CoV infection in Vero E6 cells. In SARS-infected Vero E6 cells, both incomplete activation of Akt and STAT3 dephosphorylation via p38 MAPK activation lead to apoptotic cell death. We assume that these are at least part of the mechanisms of the pathogenesis of SARS-CoV infection.

Acknowledgements: We thank Drs. F. Taguchi (National Institute of Infectious Diseases, Japan) and H. Shima, O. Inanami (Hokkaido University, Japan) for helpful suggestions. We also thank Ms. M. Ogata (National Institute of Infectious Diseases, Japan) for her assistance. This work was supported in part by a grant-in-aid from the Ministry of Health, Labor, and Welfare of Japan and the Japan Health Science Foundation, Tokyo, Japan.

References

[1] Rota, P.A., Oberste, M.S., Monroe, S.S., Nix, W.A., Campagnoli, R., Icenogle, J.P., Penaranda, S., Bankamp, B., Maher, K., Chen, M.H., Tong, S., Tamin, A., Lowe, L., Frace, M., DeRisi, J.L., Chen, Q., Wang, D., Erdman, D.D., Peret, T.C., Burns, C., Ksiazek, T.G., Rollin, P.E., Sanchez, A., Liffick, S., Holloway, B., Limor, J., McCaustland, K., Olsen-Rasmussen, M., Fouchier, R., Gunther, S., Osterhaus, A.D., Drosten, C., Pallansch, M.A., Anderson, L.J. and Bellini, W.J. (2003) Science 300, 1394–1399.
[2] Marra, M.A., Jones, S.J., Astell, C.R., Holt, R.A., Brooks-Wilson, A., Butterfield, Y.S., Khattra, J., Asano, J.K., Barber, S.A., Chan, S.Y., Cloutier, A., Coughlin, S.M., Freeman, D., Girn, N., Griffith, O.L., Leach, S.R., Mayo, M., McDonald, H., Montgomery, S.B., Pandoh, P.K., Petrescu, A.S., Robertson, A.G., Schein, J.E., Siddiqui, A., Smailus, D.E., Stott, J.M., Yang, G.S., Plummer, F., Andonov, A., Artsob, H., Bastien, N., Bernard, K., Booth, T.F., Bowness, D., Czub, M., Drebot, M., Fernando, L., Flick, R., Garbutt, M., Gray, M., Grolla, A., Jones, S., Feldmann, H., Meyers, A., Kabani, A., Li, Y., Normand, S., Stroher, U., Tipples, G.A., Tyler, S., Vogrig, R., Ward, D., Watson, B., Brunham, R.C., Krajden, M., Petric, M., Skowronski, D.M., Upton, C. and Roper, R.L. (2003) Science 300, 1399–1404.
[3] Mizutani, T., Fukushi, S., Saijo, M., Kurane, I. and Morikawa, S. (2004) Biochem. Biophys. Res. Commun. 319, 1228–1234.
[4] Mizutani, T., Fukushi, S., Saijo, M., Kurane, I. and Morikawa, S. (2004) Virology 327, 169–174.
[5] Garrington, T.P. and Johnson, G.L. (1999) Curr. Opin. Cell. Biol. 11, 211–218.
[6] Whitmarsh, A.J. and Davis, R.J. (2003) Nature 403, 255–256.
[7] Chang, L. and Karin, M. (2001) Nature 410, 37–40.
[8] Kyriakis, J.M. and Avruch, J. (2001) Physiol. Rev. 81, 807–869.
[9] Shuai, K., Stark, G.R., Kerr, I.M. and Darnell Jr., J.E. (1993) Science 261, 1744–1746.
[10] Shuai, K., Horvath, C.M., Huang, L.H., Qureshi, S.A., Cowburn, D. and Darnell Jr., J.E. (1994) Cell 76, 821–828.
[11] Shuai, K., Schindler, C., Prezioso, V.R. and Darnell Jr., J.E. (1992) Science 258, 1808–1812.
[12] Schindler, C., Shuai, K., Prezioso, V.R. and Darnell Jr., J.E. (1992) Science 257, 809–813.
[13] Rajan, P. and McKay, R.D. (1998) J. Neurosci. 18, 3620–3629.
[14] Grandis, J.R., Drenning, S.D., Zeng, Q., Watkins, S.C., Melhem, M.F., Endo, S., Johnson, D.E., Huang, L., He, Y. and Kim, J.D. (2000) Proc. Natl. Acad. Sci. USA 97, 4227–4232.
[15] Mora, L.B., Buettner, R., Seigne, J., Diaz, J., Ahmad, N., Garcia, R., Bowman, T., Falcone, R., Fairclough, R., Cantor, A., Muro-Cacho, C., Livingston, S., Karras, J., Pow-Sang, J. and Jove, R. (2002) Cancer Res. 62, 6659–6666.
[16] Palosaari, H., Parisien, J.-P., Rodriguez, J.J., Ulane, C.M. and Horvath, C.M. (2003) J. Virol. 77, 7635–7644.
[17] Thiel, V., Ivanov, K.A., Putics, A., Hertzig, T., Schelle, B., Bayer, S., Weissbrich, B., Snijder, E.J., Rabenau, H., Doerr, H.W., Gorbalenya, A.E. and Ziebuhr, J. (2003) J. Gen. Virol. 84, 2305–2315.
[18] Mizutani, T., Kobayashi, M., Eshita, Y., Shirato, K., Kimura, T., Ako, Y., Miyoshi, H., Takasaki, T., Kurane, T., Kariwa, H., Umemura, T. and Takashima, I. (2003) Insect. Mol. Biol. 12, 491–499.
[19] Garcia, R., Yu, C.-L., Hudnall, A., Catlett, R., Nelson, K.L., Smithgall, T., Fujita, D.J., Ethier, S.P. and Jove, R. (1997) Cell Growth Differ. 8, 1267–1276.
[20] Kerr, I.M., Costa-Pereira, A.P., Lillemeier, B.F. and Strobl, B. (2003) FEBS Lett. 546, 1–5.
[21] Niemand, C., Nimmesgern, A., Haan, S., Fischer, P., Schaper, F., Rossaint, R., Heinrich, P.C. and Muller-Newen, G. (2003) J. Immunol. 170, 3263–3272.
[22] Nielsen, M., Nordahl, M., Svejgaard, A. and Odum, N. (1998) Cytokine 10, 735–738.

[23] Subramaniam, S.V., Cooper, R.S. and Adunyah, S.E. (1999) Biochem. Biophys. Res. Commun. 262, 14–19.
[24] Lejeune, D., Dumoutier, L., Constantinescu, S., Kruijer, W., Schuringa, J.J. and Renauld, J.C. (2002) J. Biol. Chem. 277, 33676–33682.
[25] Haq, R., Halupa, A., Beattie, B.K., Mason, J.M., Zanke, B.W. and Barber, D.L. (2002) J. Biol. Chem. 277, 17359–17366.
[26] Chung, J., Uchida, E., Grammer, T.C. and Blenis, J. (1997) Mol. Cell. Biol. 17, 6508–6516.
[27] Liu, H., Ma, Y., Cole, S.M., Zander, C., Chen, K.H., Karras, J. and Pope, R.M. (2003) Blood 102, 344–352.
[28] Wegenka, U.M., Buschmann, J., Lutticken, C., Heinrich, P.C. and Horn, F. (1993) Mol. Cell. Biol. 13, 276–288.
[29] Yuan, J., Wegenka, U.M., Lutticken, C., Buschmann, J., Decker, T., Schindler, C., Heinrich, P.C. and Horn, F. (1994) Mol. Cell. Biol. 14, 1657–1668.
[30] Konnikova, L., Kotecki, M., Kruger, M.M. and Cochran, B.H. (2003) BMC Cancer 3, 3–23.
[31] Didcock, L., Young, D.F., Goodbourn, S. and Randall, R.E. (1999) J. Virol. 73, 9928–9933.
[32] Parisien, J.-P., Lau, J.F., Rodriguez, J.J., Sullivan, B.M., Moscona, A., Parks, G.D., Lamb, R.A. and Horvath C.M (2001) J. Virol. 283, 230–239.
[33] Nishio, M., Garcin, D., Simonet, V. and Kolakofsky, D. (2002) Virology 300, 92–99.
[34] Ulane, C.M., Rodriguez, J.J., Parisien, J.-P. and Horvath, C.M. (2003) J. Virol. 77, 6385–6393.

Available online at www.sciencedirect.com
SCIENCE DIRECT
Vaccine 23 (2005) 2269–2272
Vaccine
www.elsevier.com/locate/vaccine

The development of vaccines against SARS corona virus in mice and SCID-PBL/hu mice

Masaji Okada[a,*], Yuji Takemoto[a], Yoshinobu Okuno[b], Satomi Hashimoto[a], Shigeto Yoshida[c], Yukari Fukunaga[a], Takao Tanaka[a], Yoko Kita[a], Sachiko Kuwayama[a], Yumiko Muraki[a], Noriko Kanamaru[a], Hiroko Takai[a], Chika Okada[a], Yayoi Sakaguchi[a], Izumi Furukawa[a], Kyoko Yamada[a], Makoto Matsumoto[d], Tetsuo Kase[b], Daphne E. deMello[e], J.S.M. Peiris[f], Pei-Jer Chen[g], Naoki Yamamoto[h], Yoshiyuki Yoshinaka[h], Tatsuji Nomura[i], Isao Ishida[j], Shigeru Morikawa[k], Masato Tashiro[k], Mitsunori Sakatani[a]

[a] *Clinical Research Center, National Hospital Organization Kinki-Chuo Chest Medical Center, 1180 Nagasone, Sakai, Osaka 591-8555, Japan*
[b] *Department of Infectious Diseases, Osaka Prefectural Institute of Public Health, 3-69 Nakamichi 1-chome Higashinari-ku, Osaka 537-0025, Japan*
[c] *Department of Infection and Immunity, Jichi Medical School, 3311-1 Yakushiji, Minamikawachi-machi, Tochigi 329-0498, Japan*
[d] *Microbiological Research Institute, Otsuka Pharmaceutical Co., Ltd., 463-10, Kagasuno, Kawauchi-cho, Tokushima 771-019, Japan*
[e] *Department of Pathology Cardinal Glennon Children's Hospital, St. Louis University Health Science Center, 1465 South Grand Blvd. St. Louis, MO 63104, USA*
[f] *Department of Microbiology, The University of Hong Kong, Pokfulam Road, Hong Kong*
[g] *Hepatitis Research Center, National Taiwan University College of Medicine, Room 328, 3F, No.1, Sec. 1, Ren-ai Rd., Jhongjheng District 100, Taipei, Taiwan*
[h] *Tokyo Medical and Dental University, 1-5-45 Yushima, Bunkyo-ku, Tokyo 113-8549, Japan*
[i] *Central Institute for Experimental Animals, 1430 Nogawa, Miyamae, Kawasaki, Kanagawa 216-0001, Japan*
[j] *Pharmaceutical Division, Kirin Brewery Co., 6-26-1 Jingumae, Shibuya, Tokyo 150-8011, Japan*
[k] *National Institute of Infectious Diseases, 1-23-1 Toyama, Shinjuku-ku, Tokyo 162-8640, Japan*

Available online 21 January 2005

Abstract

We have investigated to develop novel vaccines against SARS CoV using cDNA constructs encoding the structural antigen; spike protein (S), membrane protein (M), envelope protein (E), or nucleocapsid (N) protein, derived from SARS CoV. Mice vaccinated with SARS-N or -M DNA using pcDNA 3.1(+) plasmid vector showed T cell immune responses (CTL induction and proliferation) against N or M protein, respectively. CTL responses were also detected to SARS DNA-transfected type II alveolar epithelial cells (T7 cell clone), which are thought to be initial target cells for SARS virus infection in human. To determine whether these DNA vaccines could induce T cell immune responses in humans as well as in mice, SCID-PBL/hu mice was immunized with these DNA vaccines. As expected, virus-specific CTL responses and T cell proliferation were induced from human T cells. SARS-N and SARS-M DNA vaccines and SCID-PBL/hu mouse model will be important in the development of protective vaccines.

Keywords: SARS DNA vaccine; SCID-PBL/hu; Human CTL

1. Introduction

The causative agent of severe acute respiratory syndrome (SARS) has been identified as a new type of corona virus, SARS corona virus (SARS CoV) [1–3]. SARS has infected more than 8400 patients in about 7 months in over 30 countries and caused more than 800 deaths. The deadly epidemic has had significant impacts on many health, social, economic and political aspects. SARS is assumed to resurge in the near future. However, no SARS vaccine is currently available for clinical use. Therefore, we have developed novel vaccine

* Corresponding author. Tel.: +81 72 252 3021; fax: +81 72 251 2153.
E-mail address: okm@kch.hosp.go.jp (M. Okada).

0264-410X/$ – see front matter © 2005 Elsevier Ltd. All rights reserved.
doi:10.1016/j.vaccine.2005.01.036

candidates against SARS CoV using cDNA constructs encoding the structural antigens; S, M, E, or N protein. In immunized mice, neutralizing antibodies against the virus and T cell immunity against virus-infected-cells were studied, since these immunities play important roles in protection against many virus infections. In particular, $CD8^+$ CTL plays an important role in T cell immunity dependent protection against virus infections and the eradication of murine and human cancers [4,5]. In the present study, a type II alveolar epithelial cell clone, T7, was used for analyzing precise mechanism of CTL against SARS CoV membrane antigens, as the SARS-CoV infects alveolar epithelial cell in the lungs [6]. Furthermore, the SCID-PBL/hu model, which is capable of analyzing in vivo human immune response, was also used because it is a more relevant translational model for human cases [4].

2. Materials and methods

Three kinds of SARS CoV strains: HKU39849(1), TW-1 and FFM-1(2) and their cDNAs were used. S, M, N or E cDNA was transferred into pcDNA 3.1(+) vector and pcDNA 3.1(+)/vs-His Topo (QIAGEN K K, Tokyo, Japan). These genes were expressed in eukaryotic cells and *Escherichia coli*. pcDNA 3.1(+) vector, 50 μg each, containing SARS S, M, N, or E DNA was injected i.m. (M.tibia anterior) into C57BL/6 mice (female, 8 weeks CLEA Japan Inc, Japan) and BALB/c mice (female, 8 weeks) three times, at an interval of 7 days. Neutralizing antibodies against SARS CoV in the serum from the mice immunized with SARS S, M, N or -E DNA vaccines were assayed by use of Vero-E6 cell. CTL activity against SARS CoV was studied using human type II alveolar epithelial cells, T7, expressing SARS antigens [6]. PBL from healthy human volunteers were administered i.p. into IL-2 receptor γ-chain disrupted NOD SCID mice [IL-2R(−/−) NOD-SCID], and SCID-PBL/hu mice were constructed [4]. SARS DNA vaccines at 50 μg were injected i.m. into the SCID-PBL/hu mice. CTL activity of human CD8-positive lymphocytes in the spleen from SCID-PBL/hu was assessed using IFN-γ production and 51Cr-release assay [4,5].

3. Results

3.1. Induction of CTL against SARS CoV by SARS (N) DNA and SARS (M) DNA vaccine

Spleen cells from C57BL/6 mice immunized with SARS-S, -M, -N or -E DNA vaccine were cultured with syngeneic T7 lung cells transfected with S, M, N or E cDNA. pcDNA 3.1(+) SARS (N) DNA vaccine induced significantly CTL activity (IFN-γ production) against N cDNA transfected T7 cells (Fig. 1A). Similarly, SARS M DNA vaccine induced SARS antigen M-specific CTL against T7 cells transfected with SARS M DNA (data not shown).

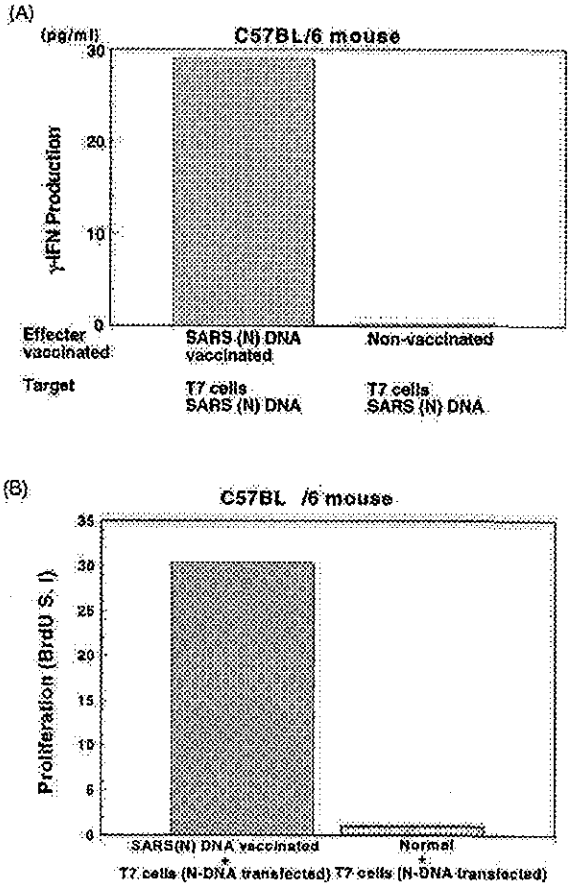

Fig. 1. Induction of CTL and T cell proliferation against SARS (N). (A) Induction of CTL against SARS (N) antigen in the spleen cells from C57BL/6 mice immunized with SARS (N) DNA vaccine. SARS (N) DNA using pcDNA3.1(+) vector was injected i.m. into C57BL/6 mice three times, at an interval of 7 days. CTL activity was assessed by IFN-γ production in the culture of 1×10^6 spleen cells and 1×10^4 T7 lung alveolar type II epithelial cells transfected with SARS (N) DNA at the E/T ratio of 100:1. IFN-γ production was assessed by ELISA assay. (B) Augmentation of lymphocyte proliferation specific for SARS (N) DNA vaccine. 1×10^5 responder cells from vaccinated mice were cultured with Mitomycin C treated 1×10^4 T7 cells transfected with SARS (N) DNA for 48 h and then Bromodeoxy Uridine (BrdU) was added. Proliferative responses were assessed by BrdU assay.

3.2. Augmentation of lymphocyte proliferation specific for SARS CoV antigens by the immunization with SARS (M) DNA and SARS (N) DNA vaccine

The proliferation of splenic T cells stimulated by co-culture either with T7 cells transfected with M DNA or SARS M peptide (TW1 M102-116) was strongly augmented by M DNA vaccine (data not shown). SARS N DNA vaccine also induced proliferation of splenic T cells in the presence of recombinant N protein as well as N DNA-transfected T7 cells (Fig. 1B). Thus, both SARS N DNA vaccine and

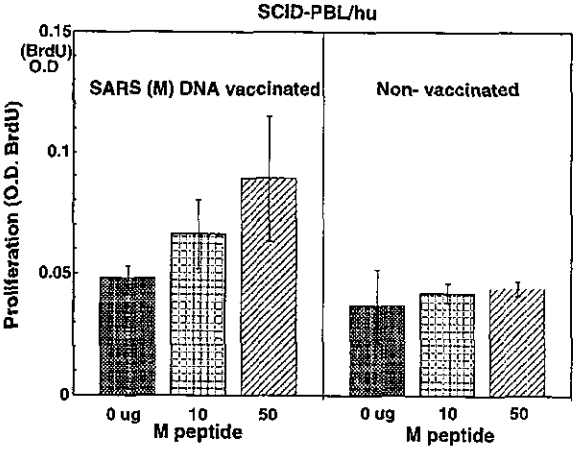

Fig. 2. SARS (M) DNA vaccine induces in vivo human T cell proliferation against SARS CoV in the SCID-PBL/hu human immune systems. 4×10^7 PBL from healthy human volunteers were administered i.p. into IL-2 receptor γ-chain disrupted NOD SCID mice [IL-2R (−/−) NOD-SCID], and SCID-PBL/hu mice were constructed. Fifty micrograms of SARS DNA vaccine was injected i.m. into these SCID-PBL/hu mice. 1×10^5 spleen cells from these vaccinated mice were cultured with 10~50 μg of SARS M peptide for 3 days. Proliferation was assayed by BrdU.

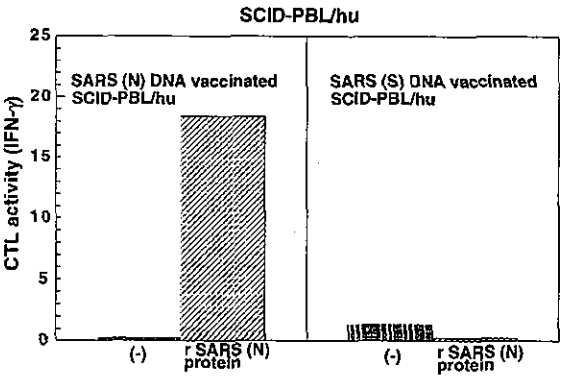

Fig. 3. SARS (N) DNA vaccine induces in vivo human CTL against SARS CoV in the SCID-PBL/hu human immune systems. 4×10^7 PBL from healthy human volunteers were administered i.p. into IL-2 receptor γ-chain disrupted NOD SCID mice [IL-2R (−/−) NOD-SCID], and SCID-PBL/hu mice were constructed 50 μg of SARS (N) DNA vaccine or 50 μg of SARS (S) DNA vaccine. 1×10^5 spleen cells from SCID-PBL/hu were cultured with 10 μg of recombinant SARS (N) protein for 72 h. IFN-γ production in the culture supernatant was assayed using ELISA.

M DNA vaccine were shown to induce T cell immune responses against the relevant SARS CoV antigens.

3.3. SARS M DNA and N DNA vaccines induced human T cell immune responses (CTL and proliferation) in SCID-PBL/hu model

The M DNA vaccine enhanced the CTL activity and proliferation in the presence of M peptide in SCID-PBL/hu mice (Fig. 2). Furthermore, the SARS N DNA vaccine induced CTL activity (IFN-γ production by recombinant N protein or N protein pulsed-autologous B blast cells) and proliferation of spleen cells in SCID-PBL/hu mice (Fig. 3). From these results, it was demonstrated that SARS M DNA vaccine and N DNA vaccine induced human CTL and human T cell proliferative responses.

4. Discussion

We have demonstrated that SARS (M) DNA and (N) DNA vaccines induce virus-specific immune responses (CTL and T cell proliferation) in the mouse systems using type II lung alveolar T cell lines in clone target models [6]. These DNA vaccines induced SARS-CoV-specific CTL and T cell proliferation in vivo human immune systems using SCID-PBL/hu. Gao et al. developed adenovirus based a SARS DNA vaccine encoding S1 polypeptide was capable of inducing neutralizing antibody, while another SARS DNA vaccine encoding N protein generated IFN-γ producing T cells in rhesus monkeys [7]. SARS S DNA vaccine which elicits effective neutralizing antibody responses that generate protective immunity in a mouse model [8]. However its immunogenicity in humans has yet to be established. Therefore, it is very important to evaluate the efficacy of SARS DNA vaccine in a SCID-PBL/hu mice, which is a highly relevant translational model for demonstrating human immune responsiveness. Recently, SARS DNA vaccines capable of inducing human neutralizing antibodies against SARS CoV have been established by our SCID-PBL/hu model. It has been demonstrated that Angiotensin-converting enzyme 2 (ACE2) is a functional receptor for the SARS CoV [9]. A transgenic mouse with human ACE-2 may be useful as an animal model of SARS. Furthermore, ACE-2 transgenic SCID mice should be useful as a human model for pre-clinical trial for SARS vaccines, since ACE-transgenic SCID-PBL/hu model could analyze the human immune responses against SARS infection in vivo. The effect of combination immunization with such SARS vaccines and neutralizing antibody dependent DNA vaccine is now being studied. These DNA vaccines should provide a useful tool for development of protective vaccines.

Acknowledgements

This study was supported by Grant-in-Aid for the science and technology and Grant-in-Aid for Scientific Research on Priority Areas from the Ministry of Education Culture Sports, Science and Technology, Japan. This study was also supported by a Heath and Labour Science Research Grant from the Ministry of Health, Labour, and Welfare, Japan.

References

[1] Peiris JS, Lai ST, Poon LL, Guan Y, Yam LY, Lim W, et al. SARS study group. Coronavirus as a possible cause of severe acute respiratory syndrome. Lancet 2003;361(9366):1319–25.

[2] Drosten C, Gunther S, Preiser W, van der Werf S, Brodt HR, Becker S, et al. Identification of a novel coronavirus in patients with severe acute respiratory syndrome. N Engl J Med 2003;348(20):1967–76.
[3] Peiris JS, Yuen KY, Osterhaus AD, Stohr K. The severe acute respiratory syndrome. N Engl J Med 2003;349(25):2431–41.
[4] Tanaka F, Abe M, Akiyoshi T, Nomura T, Sugimachi K, Kishimoto T, et al. The anti-human tumor effect and generation of human cytotoxic T cells in SCID mice given human peripheral blood lymphocytes by the in vivo transfer of the Interleukin-6 gene using adenovirus vector. Cancer Res 1997;57(7):1335–43.
[5] Okada M, Yoshimura N, Kaieda T, Yamamura Y, Kishimoto T. Establishment and characterization of human T hybrid cells secreting immunoregulatory molecules. Proc Natl Acad Sci USA 1981;78(12):7717–21.
[6] deMello DE, Mahmoud S, Padfield PJ, Hoffmann JW. Generation of an immortal differentiated lung type-II epithelial cell line from the adult H-2K(b)tsA58 transgenic mouse. In Vitro Cell Dev Biol Anim 2000;36(6):374–82.
[7] Gao W, Tamin A, Soloff A, D'Aiuto L, Nwanegbo E, Robbins PD, et al. Effects of a SARS-associated coronavirus vaccine in monkeys. Lancet 2003;362(9399):1895–6.
[8] Yang ZY, Kong WP, Huang Y, Roberts A, Murphy BR, Subbarao K, et al. A DNA vaccine induces SARS coronavirus neutralization and protective immunity in mice. Nature 2004;428(6982):561–4.
[9] Li W, Moore MJ, Vasilieva N, Sui J, Wong SK, Berne MA, et al. Angiotensin-converting enzyme 2 is a functional receptor for the SARS coronavirus. Nature 2003;426(6965):450–4.

International Immunology, Vol. 16, No. 10, pp. 1423–1430
doi:10.1093/intimm/dxh143 Advance Access publication 16 August 2004

A subcutaneously injected UV-inactivated SARS coronavirus vaccine elicits systemic humoral immunity in mice

Naomi Takasuka[1], Hideki Fujii[1], Yoshimasa Takahashi[1], Masataka Kasai[1], Shigeru Morikawa[2], Shigeyuki Itamura[4], Koji Ishii[3], Masahiro Sakaguchi[1], Kazuo Ohnishi[1], Masamichi Ohshima[1], Shu-ichi Hashimoto[1], Takato Odagiri[4], Masato Tashiro[4], Hiroshi Yoshikura[5], Toshitada Takemori[1] and **Yasuko Tsunetsugu-Yokota[1]**

[1]Department of Immunology, [2]First, [3]Second and [4]Third Departments of Virology, [5]National Institute of Infectious Diseases, Toyama 1-23-1, Shinjuku-ku, Tokyo 162-8640, Japan

Keywords: alum, cellular immunity, neutralizing antibody, parenteral administration, vaccination

Abstract

The recent emergence of severe acute respiratory syndrome (SARS) was caused by a novel coronavirus, SARS-CoV. It spread rapidly to many countries and developing a SARS vaccine is now urgently required. In order to study the immunogenicity of UV-inactivated purified SARS-CoV virion as a vaccine candidate, we subcutaneously immunized mice with UV-inactivated SARS-CoV with or without an adjuvant. We chose aluminum hydroxide gel (alum) as an adjuvant, because of its long safety history for human use. We observed that the UV-inactivated SARS-CoV virion elicited a high level of humoral immunity, resulting in the generation of long-term antibody secreting and memory B cells. With the addition of alum to the vaccine formula, serum IgG production was augmented and reached a level similar to that found in hyper-immunized mice, though it was still insufficient to elicit serum IgA antibodies. Notably, the SARS-CoV virion itself was able to induce long-term antibody production even without an adjuvant. Anti-SARS-CoV antibodies elicited in mice recognized both the spike and nucleocapsid proteins of the virus and were able to neutralize the virus. Furthermore, the UV-inactivated virion induced regional lymph node T-cell proliferation and significant levels of cytokine production (IL-2, IL-4, IL-5, IFN-γ and TNF-α) upon restimulation with inactivated SARS-CoV virion *in vitro*. Thus, a whole killed virion could serve as a candidate antigen for a SARS vaccine to elicit both humoral and cellular immunity.

Introduction

A new disease called severe acute respiratory syndrome (SARS) originated in China in late 2002 and spread rapidly to many countries. Upon this outbreak, a global collaboration network was coordinated by WHO. As a result of this unprecedented international effort, a novel type of coronavirus (SARS-CoV) was identified as the etiologic agent of SARS (1,2) in March 2003. The genomic sequence of SARS-CoV was completed and we now know that SARS-CoV has all the features and characteristics of other coronaviruses, but it is quite different from all previously known coronaviruses (groups I~III), representing a new group (group IV) (3,4). It is assumed that SARS-CoV is a mutant coronavirus transmitted from a wild animal that developed the ability to productively infect humans (3,5). The genome of SARS-CoV is a single-stranded plus-sense RNA ~30 kb in length and containing five major open reading frames that encode nonstructural replicase polyproteins and structural proteins: the spike (S), envelope (E), membrane (M) and nucleocapsid protein (N), in the same order and of approximately the same sizes as those of other coronaviruses (5).

The reason why SARS-CoV induces severe respiratory distress in some, but not all, infected individuals is still unclear. In patients with SARS and probable SARS cases, virus is detected in sputum, stool and plasma by RT-PCR (1,2). These patients developed serum antibodies against SARS-CoV and high antibody titers against N protein were maintained for more than 5 months after infection (6). Because of their generally poor pathogenicity and difficulty of propagation

Correspondence to: Y. Tsunetsugu-Yokota; E-mail: yyokota@nih.go.jp

Transmitting editor: K. Sugamura

Received 6 May 2004, *accepted* 15 July 2004

in vitro, there have been few studies regarding immunity to human coronaviruses OC43 and 229E. In the veterinary field, however, coronaviruses have been known for many years to cause a variety of lung, liver and gut diseases in animals. As we learned from these animal models, both humoral and cellular immune responses may contribute to protection against coronavirus diseases, including SARS [for review see (7)].

The clinical manifestation of SARS is hardly distinct from other common respiratory viral infections including influenza. Because an influenza epidemic may occur simultaneously with the re-emergence of SARS, it is urgently required that we develop effective SARS vaccines as well as sensitive diagnostic tests specific for SARS. Recently, the angiotensin-converting enzyme 2 (ACE2) was identified as a cellular receptor for SARS-CoV (8). The first step in viral infection is presumably the binding of S protein to its receptor, ACE2. In the murine MHV model, S proteins are known to contain important virus-neutralizing epitopes that elicit neutralizing antibodies in mice (9,10). Therefore, the S protein would be the first candidate coronavirus protein for induction of immunity. However, the S, M and N proteins are also known to contribute to generating the host immune response (11,12).

Following an established vaccine protocol is one of the best ways to shorten the time and cost of new vaccine development. Most of the currently available vaccines for humans are inactivated and applied cutaneously, except oral polio vaccine, and adjuvant usage is mostly limited to aluminum hydroxide gel (alum). In order to know the immunogenicity of inactivated SARS-CoV as a vaccine candidate, we immunized mice with UV-inactivated SARS-CoV either with or without alum. We report here the evaluation of humoral and cellular immunity elicited by UV-inactivated SARS-CoV administered subcutaneously.

Methods

Preparation of UV-inactivated purified SARS-CoV

SARS-CoV (HKU39849) was kindly supplied by Dr J.S.M. Peiris, Department of Microbiology, The University of Hong Kong. The virus was amplified in Vero E6 cells and purified by sucrose density gradient centrifugation. Concentrated virus was then exposed to UV light (4.75 J/cm^2) in order to inactivate the virus. We confirmed that the virus completely lost its infectivity by this method.

Immunization of mice

Female BALB/c mice were purchased from Nippon SLC Inc. (Shizuoka, Japan) and were housed under specific pathogen-free conditions. All experimental procedures were carried out under NIID-recommended guidelines. Mice were subcutaneously injected via their back or right and left hind leg footpads with 10 μg of UV-inactivated purified SARS-CoV with or without 2 mg of alum, and boosted by the same procedure 7 weeks after priming.

Detection of immunoglobulins in the serum samples

Blood was obtained from the tail vein and allowed to clot overnight at 4°C. Sera were then collected by centrifugation. For ELISA, microtiter plates (Dynatech, Chantily, VA) were coated overnight at 4°C with SARS-CoV-infected or mock-infected Vero E6 cell lysates, which had been treated with 1% NP40 followed by UV-inactivation. To detect S or N protein, the plates were coated with 1% NP40 lysates of chick embryo fibroblasts that had been infected with S or N protein-expressing DIs (attenuated vaccinia virus) (13). The plates were blocked with 1% OVA in PBS–Tween (0.05%) and then incubated with the sera serially diluted at 1:25–1:10^5 for 1 h at room temperature. Plates were incubated with either peroxidase-conjugated anti-mouse IgG (1:2000, Zymed, San Francisco, CA), IgM or IgA (1:2000, Southern Biotechnology, Birmingham, AL) antibody. For detection of IgG subclasses, either peroxidase-conjugated anti-mouse IgG_1, IgG_{2a}, IgG_{2b} (1:2000, Zymed) or IgG_3 (1:2000, Southern Biotechnology) was used. Plates were washed three times with PBS–Tween at each step. Antibodies were detected by *O*-phenylenediamine (Zymed), and the absorbance of each well was read at 490 nm using a model 680 microplate reader (Bio-Rad, Hercules, CA). As a standard for IgG detection, serum was obtained from a hyper-immunized mouse; the OD490nm value of 100 U/ml standard was ~3 in all assays. SARS-CoV-specific IgG titer was calculated as follows: SARS-specific IgG titer (U/ml) = (the unit value obtained at wells coated with virus-infected cell lysates) – (the unit value obtained at wells coated with non-infected cell lysates).

ELISPOT assay for antibody-secreting cells (ASCs)

Recombinant N protein (amino acids 1–49 and 340–390) of SARS-CoV (Biodesign, Saco, ME) was diluted to 10 μg/ml in PBS, and then added at 100 μl per well to plates supported by a nitrocellulose filter (Millipore, Bedford, MA). After overnight incubation at 4°C, the plates were washed with PBS three times and then blocked at 4°C overnight with 1% OVA in PBS–Tween (0.05%). After erythrocyte lysis, single cell suspensions from BMs were suspended in RPMI supplemented with 10% FCS, 5 × 10^{-5} M 2ME, 2 mM L-glutamine, 100 U/ml penicillin and 100 μg/ml streptomycin, and then applied to the plates at a concentration of 3 × 10^5 cells per well. After 24 h cultivation, the plates were recovered and stained with alkaline phosphatase-conjugated anti-mouse IgG_1 antibody (Southern Biotechnologies). Alkaline phosphatase activity was visualized using 3-amino-ethyl carbozole and napthol AS-MX phosphate/fast blue BB (Sigma). The frequency of plasma cells specific for N protein was determined from the N protein-coated plates after background on the uncoated plates was subtracted.

Coronavirus neutralizing assay

Serum was inactivated by incubation at 56°C for 30 min. The known tissue culture infectious dose (TCID) of SARS-CoV was incubated for 1 h in the presence or absence of serum antibodies serially diluted 5-fold, and then added to Vero E6 cell culture grown confluently in a 96-well microtiter plate. After 48 h, cells were fixed with 10% formaldehyde and stained with crystal violet to visualize the cytopathic effect induced by the virus (14). Neutralization antibody titers were expressed as the minimum dilution number of serum that inhibited the cytopathic effect.

Western blotting

Purified SARS-CoV virion (0.5 μg) was fractionated on SDS–PAGE under reduced conditions. Proteins were transferred to PVDF membrane (Genetics, Tokyo, Japan) and reacted with the diluted sera (1:1000) that had been obtained from mice inoculated with UV-irradiated SARS-CoV. After washing, the membrane was reacted with HRP-conjugated $F(ab')_2$ fragment anti-mouse IgG (H+L) (1:20 000 Jackson Immuno Research, West Grove, PA), followed by visualization of the bands on X-ray film (Kodak, Rochester, NY) using chemiluminescent regents (Amasham Biosciences, Piscataway, NJ).

Regional T cell response

Popliteal and inguinal lymph nodes and spleens were harvested from mice 1 week after the boost vaccination. After the preparation of a single cell suspension, T cells were purified by depletion of $B220^+$, $Gr1^+$, $CD11b^+$, IgD^+ and IgM^+ cells using a magnetic cell sort system (MACS: Miltenyi Biotec, Bergisch Gladbach, Germany). To prepare antigen-presenting cells (APC), normal BALB/c mouse splenocytes were depleted of $CD3^+$ T cells by MACS and irradiated at 2000 cGy.

Purified T cells taken from lymph nodes (1×10^5 cells/well) were cultured with irradiated APC (5×10^5 cells/well) in the presence or absence of UV-irradiated purified SARS-CoV virion (1 or 10 μg/ml). Four days after the cultivation, the level of cytokine concentration in the culture supernatant was measured by flow cytometry using a mouse Th1/Th2 cytokine cytometric bead array kit (Becton Dickinson, San Jose, CA). T-cell proliferation was monitored by the incorporation of [^{3}H]thymidine (18.5 kBq/well, ICN Biomedicals, Costa Mesa, CA) added 8 h prior to cell harvest. The cells were harvested on a 96-well microplate bonded with a GF/B filter (Packard Instruments, Meriden, CT). Incorporated radioactivity was counted by a microplate scintillation counter (Packard Instruments).

Results

Inoculation with UV-inactivated SARS-CoV results in an antigen-specific IgG_1 response, probably by generating long-term ASCs as well as memory cells

To examine the level of anti-SARS-CoV response in mice after inoculation with vaccine candidates, three mice in each group were subcutaneously inoculated with 10 μg of UV-inactivated purified SARS-CoV with (Virion/Alum) or without alum (Virion), or inoculated with alum alone (Alum) or left untreated (None) as a control (Fig. 1). One month after inoculation, vaccinated mice elicited the anti-SARS CoV IgG antibody in sera at high levels. As expected, the alum adjuvant enhanced the level of IgG antibody response, >10-fold higher than the level without adjuvant (Fig. 1C compared with B). When mice were boosted at 7 weeks, the level of IgG antibody in both groups of mice was further increased ~10-fold above the primary response (Fig. 1B and C). Notably, the level of serum antibodies induced by a single injection of virion, even in the absence of the alum adjuvant, was maintained at least more than 6 months (Fig. 1D). These results suggest that long-term ASCs can be established by a single shot of UV-inactivated virion administration.

Upon restimulation with antigen, memory B cells rapidly differentiate into ASCs and migrate into the bone marrow to establish a long-term ASC pool (15,16). To enumerate the number of plasma cells specific for SARS-CoV, we performed an ELISPOT assay using recombinant N proteins, amino acid numbers 1–49 (N1–49) and 340–390 (N340–390) as coating antigens. Consistent with the serum anti-SARS CoV IgG level, SARS-specific IgG_1 plasma cells were maintained in the bone marrow at day 10 after boost immunization with virion/alum

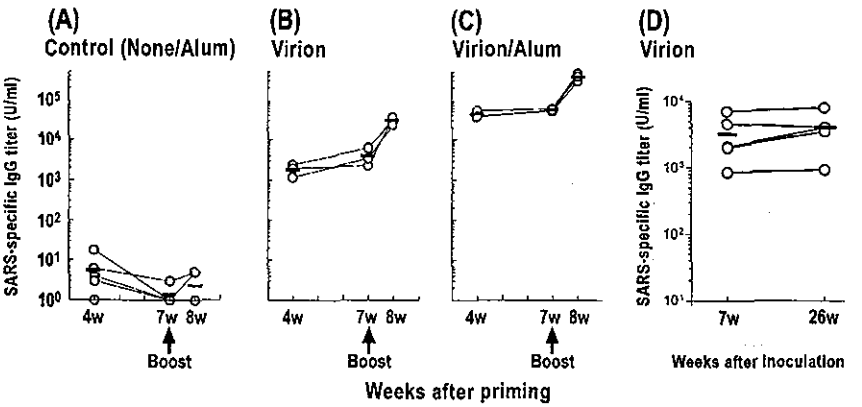

Fig. 1. The level of SARS-specific IgG in subcutaneously vaccinated mice. Mice were subcutaneously primed with 10 μg of UV-inactivated SARS-CoV virion (B), or virion with 2 mg of alum (C), or alum alone or none (A) and boosted with the same dose in their footpads at 7 weeks after priming. Serum was collected at the indicated time point and subjected to ELISA to detect SARS-specific IgG using SARS-CoV-infected Vero cell lysates as a coating antigen. Circles and bars represent the amount of IgG antibody in the serum of each mouse and the mean, respectively. The amount of IgG was arbitrarily calculated based on the concentration of hyper-immune sera. A representative result of two independent experiments is shown. (D) Mice were vaccinated with 10 μg of UV-inactivated SARS-CoV virion subcutaneously into their backs. Serum was collected from individual mice at the indicated time point and subjected to ELISA to detect SARS-specific IgG.

(Fig. 2). In contrast, the number of spots from control mice was below the detection limit (i.e. <1 ASC/9 × 10^5 cells).

UV-inactivated SARS-CoV induces IgG_1 antibody with neutralizing activity

We determined the subclass of serum anti-SARS-CoV IgG antibodies in the boosted mice using anti-mouse IgG_1, IgG_{2a}, IgG_{2b} or IgG_3 second antibody by ELISA (Fig. 3). Interestingly, the level of anti-SARS-CoV IgG_{2a} in mice immunized with virion/alum was comparable to that in mice immunized with virion alone, whereas the level of anti-SARS-CoV IgG_1 was higher in mice with virion/alum than the mice with virion alone. In contrast, the levels of IgG_{2b} and IgG_3 antibodies were fairly low in both groups. Therefore, our results indicated that vaccination with a combination of inactivated virion and alum induced a predominantly Th2-type immune response.

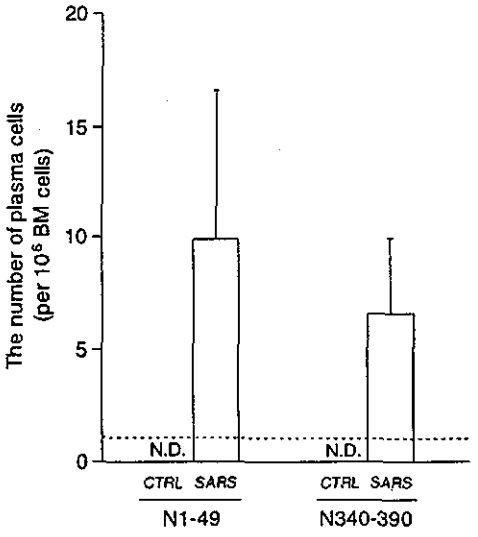

Fig. 2. The number of SARS-specific IgG_1 plasma cells in BM. Mice were primed and boosted by subcutaneous injection into their back with 10 μg of UV-inactivated SARS-CoV virion with 2 mg of alum (VA). BMs were collected at 10 days after boost and subjected to ELISPOT to detect SARS-specific IgG_1 plasma cells. Bars represent the number of plasma cells specific to N1–49 and N340–390 antigen in SARS-vaccinated and control mice, respectively. Data are means of triplicate cultures. The number of spots from control mice was below the detection limit (i.e. <1 ASC/9 × 10^5 cells: dashed line). A representative result of two independent experiments is shown. N.D.: not detected.

We also measured serum immunoglobulins other than IgG in the early and late phases of immunization. To avoid high IgG concentrations interfering with the detection of IgM and IgA antibodies, the serum IgG was absorbed with protein G-conjugated beads (>98%). The levels of anti-SARS-CoV IgM antibodies in the IgG-depleted sera, which were obtained 4 weeks after priming, were below our detection limit. Likewise, anti-SARS-CoV IgA antibody in the IgG-depleted sera, which were obtained 1 week after booster, was not detectable (data not shown).

Whether or not immune sera possess a neutralizing activity against SARS-CoV is a crucial aspect of vaccination. We estimated the neutralizing activity of sera obtained 1 week after boost inoculation (Table 1). We observed that neutralizing activity against SARS-CoV was detected at a high level in sera of mice inoculated with virion/alum or virion alone. Taken together, these results indicate that subcutaneous vaccination with UV-inactivated SARS-CoV virion is able to elicit a sufficient amount of IgG antibodies with neutralizing activity.

UV-inactivated SARS-CoV induces serum IgG antibody specific for S and N proteins

Using the immune sera of mice boosted with virion/alum 1 week before, we analyzed the specificity of serum IgG by western blot analysis (see Methods). As shown in Fig. 4(A), the robust signal detected at 50 kDa corresponds to the N protein of SARS-CoV, as predicted by its genome size (3,4). A band near 200 kDa appears to correspond to S protein, analogous with the S protein of other human coronaviruses, HCV-229E

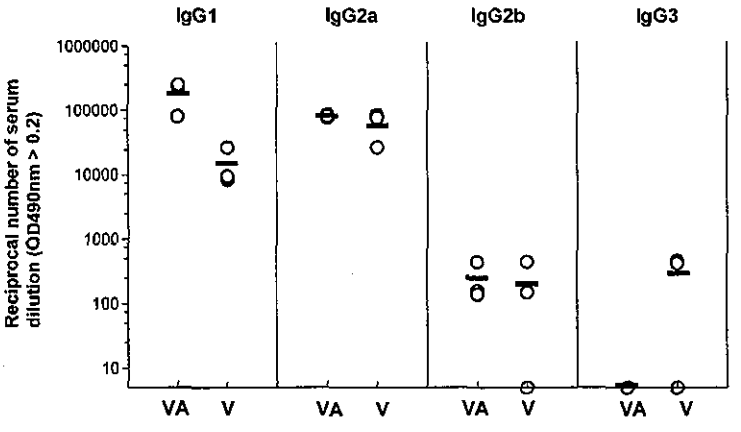

Fig. 3. IgG subclass of immunized serum. Mice were subcutaneously primed and boosted by injection in their footpads with 10 μg of UV-inactivated SARS-CoV virion (V), or virion with 2 mg of alum (VA). Serum was collected from individual mice at 1 week after boost and subjected to ELISA to detect SARS-specific IgG_1, IgG_{2a}, IgG_{2b} and IgG_3 titer. The Y value is the reciprocal serum dilution number where the OD490nm ≥ 0.2 in each ELISA. Circles and bars represent the titer for each mouse and the mean, respectively; results are representative of two separate experiments.